ELECTRIC INFRARED DIE HEATING FOR ALUMINUM HIGH PRESSURE DIE CASTING

by

Carl Shi

A Thesis

Submitted to the Faculty of Purdue University

In Partial Fulfillment of the Requirements for the Degree of

Master of Science

School of Engineering Technology

West Lafayette, Indiana

December 2020

THE PURDUE UNIVERSITY GRADUATE SCHOOL
STATEMENT OF COMMITTEE APPROVAL

Dr. Jason Ostanek, Chair

    Department of Engineering Technology

Dr. Milan Rakita

    Department of Engineering Technology

Dr. Xiaoming Wang

    Department of Engineering Technology

Mr. Corey Vian

    FCA Group

Approved by:

    Dr. Duane D. Dunlap

        Head of the Graduate Program, School of Engineering Technology

Dedicated to my family, who have always supported my decisions in life.

ACKNOWLEDGMENTS

I would like to thank to my advisor, Dr. Jason Ostanek for providing me with the opportunity to conduct this research, and his ongoing help in my research and academic endeavors. I wish to gratefully acknowledge my thesis committee for their insightful comments and guidance. I would like to thank my family for their support and encouragement. I would like to thank visiting scholar, Luis Carlos Maldonado Jaime for all his input and help on conducting the experiment and his efforts in software simulations for the project. I would like to thank the lab engineer Clayton Kibbey, for providing help during the setup of our experiment apparatus, and his help in machining our die.

Finally, I would like to acknowledge the support from Fiat Chrysler Automobiles, as they provided us with the financial support needed for this project. I am also grateful for the help provided throughout the project by Corey Vian from the Fiat Chrysler Automobiles Kokomo Casting plant located in Kokomo, Indiana.

TABLE OF CONTENTS

LIST OF FIGURES

LIST OF TABLES

LIST OF ABBREVIATIONS

AISI   American Iron and Steel Institute Standard

FCA   Fiat Chrysler Automobiles

HPDC   High Pressure Die Casting

I/O   Input/Output

IR   Infrared Radiation

SS   Stainless Steel

TC   Thermocouple

LWIR   Long Wave Infrared Radiation

MWIR   Medium Wave Infrared Radiation

SWIR   Short Wave Infrared Radiation

NOMENCLATURE

Symbols:

A – Surface area, m^2

b – Constant of proportionality, μm·K

c_p – Specific heat, J/kg

F – View factor

Fo – Thermal Fourier number

H – Thickness of die, m

k – Thermal conductivity, W/m·K

L – Thickness of slab

P – Power, kW

q – Heat flux, kW/m^2

$\tilde{q}$ – Dimensionless heat flux variable

t – Characteristic time, s

$\tilde{t}$ – Dimensionless time variable

T – Temperature, K

$\tilde{T}$ – Dimensionless temperature variable

x – Distance measured from heater surface into the material

$\tilde{x}$ – Dimensionless position variable

X – Length of die surface, m

$\overline{X}$ – Dimensionless length of variable

Y – Width of die surface, m

$\overline{Y}$ – Dimensionless width variable

Greek:

α – Thermal diffusivity, m^2/s

λ – Spectral wavelength, μm

ρ – Density, kg/m^2

ρ_r – Reflectance

GLOSSARY

80/20 – Standardized aluminum multipurpose framing for generally used for custom
mounting and assembly

Infrared – Electromagnetic radiation with longer wavelengths than those of visible light

Visible Light – Electromagnetic waves with wavelengths ranging approximately 380 nm -
780 nm [1]

LWIR – Infrared radiation with wavelengths ranging 3.00 μm - 1 mm [1]

MWIR – Infrared radiation with wavelengths ranging 1.50 μm - 3.00 μm [1]

SWIR – Infrared radiation with wavelengths ranging 0.78 μm - 1.50 μm [1]

ABSTRACT

Author: Shi, Carl. M.S.
Institution: Purdue University
Degree Received: December 2020
Title: Electric Infrared Die Heating for Aluminum High Pressure Die Casting
Major Professor: Jason Ostanek

Casting is a substantial part of modern manufacturing and production, typically used in the production of aluminum alloys. The high pressure die casting process is extremely suitable for mass production. Due to the high volume, wasted time and resources during the production cycle become more significant. Aluminum die castings require the die to be at elevated temperatures to produce acceptable castings. When the inner surfaces of a die are cold, the outer shell of the casting will cool too rapidly, and solidification of the outer shell occurs before the aluminum has time to uniformly fill the cavities. Therefore, without the die being within the proper temperature range, the castings produced will have significant issues in porosity and casting incompleteness. Furthermore, stresses are introduced to the casting surfaces when warm-up shots are used to raise the temperature prior to production. In the present work, research is conducted on designing a heating method for a casting die used in the manufacturing of an automotive transmission intermediate plate. An electric, short wave infrared heating system is simple and effective for the purpose. By utilizing an electric infrared heater in combination with a flat mirror reflector, the aluminum high pressure die casting die was heated to 300 °C surface temperature within 30 minutes. Further research can be done to optimize heat flux distribution and minimize energy consumption.

CHAPTER 1. INTRODUCTION

Chapter 1 provides an overview on the topic of heating dies used in aluminum high pressure die casting (HPDC). The problem is defined, and the project scope, assumptions, limitations, and delimitations are discussed.

1.1 Problem Statement

The current automotive industry relies heavily on the use of HPDC for manufacturing aluminum alloy components. This is a manufacturing method that has the ability to reliably conduct high volume production of aluminum alloy products of varying sizes and complexity with the use of a die. Simplifying its process, HPDC generally consists of four procedures: First, molten metal is fed into a shot sleeve, second, a piston forces the metal into the die cavity, third, pressure is maintained in the cavity as the casting cools and hardens, lastly, the finished casting is ejected as the die opens [2].

The die casting process scales well for mass production, however initial costs for hardware and equipment are high, and to achieve the optimum effectiveness of this manufacturing method, dies must be run in continuous repeated cycles maintaining a quasi-steady equilibrium state. At initial startup of a production process, the die is usually well below the required temperature range, unusable for normal production. Performing casting cycles under this condition results in the rapid cooling of the injected aluminum, in which will solidify before filling the die cavity completely, leading to an end product with a multitude of defects, including but not limited to poor surface finishes and high internal porosity [3].

A typical strategy to heat the die is to perform a number of casting cycles to warm the die before production begins. These cycles are nearly identical to production runs with few differences to assist in the warm-up procedure, such as the use of warm-up die lubricant. The castings during these cycles are scrapped, since they only serve as byproducts of the warm-up procedure. Although this method can successfully warm the die, it consumes raw material turning them into unusable castings. Furthermore, it also introduces high thermal stress on the dies when hot aluminum is brought into contact with a cold die. This significantly increases the wear and tear on the dies, resulting in reduced service life and increased operating costs of these components [3].

A solution to improve the warm-up process is to introduce an alternative heating method that is capable of replacing the function of warm-up casting cycles, able to heat the die to its quasi-steady temperature range while keeping the time spent on warm-up relatively comparable. Additional functionality, such as maintaining die temperature during production downtime can also become a potential application in improving overall operating efficiency of the HPDC process.

1.2 Research Question

The research question to be answered in this work is: how effective is an electric short wave infrared (SWIR) auxiliary heater in heating an H13 aluminum HPDC die? The heating effectiveness will be assessed by measuring the time required to heat the surface of the die from ambient temperature to 300 °C. An acceptable heating time is defined as 30 minutes or less.

1.3 Project Scope

At the beginning of this project, various types of heating methods that could be used were researched and compared, and an appropriate option to perform the task of heating a HPDC die was selected. The selection was set on an electric SWIR preheating system, heater requirements were determined, and a prototype heater was purchased. An experiment was designed around the evaluation of heater performance on an automotive transmission intermediate plate die. Experiments were conducted, and results were recorded for analysis to quantify the performance of the heating system.

1.4 Significance of the Problem

Aluminum HPDC is a common manufacturing process that the modern automotive industry heavily relies on. Most vehicles manufactured in the modern age all contain a significant amount of cast aluminum components [4]. A great number of drive-train, structural components, and some body panels (e.g. engine blocks, transmission casings, control arms etc.) are mass produced using aluminum HPDC [4]. Given the high production volume of aluminum HPDC components, improvements in the overall process will bring enormous cost and time savings for a production plant, which consecutively will bring heightened productivity and profit [4].

Currently, to the author's knowledge, industry mainly relies on the practice of injecting multiple shots of molten aluminum into cold dies to warm them prior to production [3]. This method, albeit effective, creates great thermal shock and stress on the die itself, lowering the die's life significantly due to accelerated crack formation on the die material. It also occupies valuable production time and resources, through interviewing FCA, it was stated that, "in general 10% of the cycles made go to warm up scrap". [3]

One method for preheating a die is to have it removed from the casting machine and placed inside a furnace/oven prior to production cycles. This is a common method used in hot forging, where the billets are heated prior to forging [5]. However, this would be rather unfeasible for the use in HPDC, as the added equipment and transport times required would defeat the purpose of having such a system. The system should be flexible and minimize impact on the production cycles. This objective can be better achieved with the use of auxiliary systems that can be utilized during the production cycle. Such systems can be constructed via a variety of methods, depending on the desired functions and end goals of the user, infrared, direct flame, induction and resistance etc. may all be potential methods that can be considered.

Conclusively, feasible and effective preheating methods have not been fully employed for HPDC, especially ones that have the ability to provide heating to the dies during the manufacturing process. This allows an opportunity to look further into the feasibility and cost associated with implementations of such systems.

1.5 Assumptions

The assumptions for this research are:

- Die can be opened to any arbitrary spacing.

- Horizontal orientation of the heater will perform similarly to a vertical orientation.

- Heat losses to conduction and convection of the exposed surfaces around and under the die are minimal compared to the radiation heat flux at the surface.

- TC installation does not affect the heat flow within the die.

- The die is constructed with a single material with consistent properties.

- Humidity and ambient temperature variation is negligible on heater performance.

1.6 Limitations

The limitations for this research are:

- Die casting surface geometry is fixed and cannot be altered. Protruding features on the die surface may cause hot spots or shadowing on specific regions of the die.

- Die is highly conductive. Heat is quickly transferred away from the surface and into the bulk material.

- Die mass is large. Heating time required is increased due to the large thermal mass.

- Top of the die surface cannot be insulated. Natural convection will dissipate some of the heat and increase heating time required.

- Standoff distance minimum value is limited by elevated features on the die surface. Closer standoff distances would effectively increase the surface heat flux hence reduce the heating time.

1.7 Delimitations

The delimitations for this research are:

- Heating is performed on one half of the complete die assembly provided.

- Heating is performed in the horizontal orientation, with the die and heater both sitting flat relative to the mounting surface and parallel to one another.

- Only the die core is present, external housings and cooling lines are nonexistent.

- Coolant effects are not accounted for as they are absent in this study.

- There are multiple open holes going through the die where the ejector plate is absent.

- Optical properties of the die surface are neither altered nor modified. This better represents an actual die surface in a production environment.

1.8 Summary

The problem that this research project is aimed to tackle is the improvement of the preheating process of the dies used for aluminum die casting. Being a widely implemented in the industry for manufacturing cast aluminum products, it has the ability to produce high quality parts in bulk reliably and consistently. However, dies used in this process need to be operating within their designed operating temperatures in order to achieve optimal performance. Without satisfying this condition, castings produced will be defective. Thus, a preheating process is unavoidable for users of this manufacturing process. The traditional preheating method is to utilize the heat transfer from injected molten metal to raise die temperature rapidly through warm-up casting cycles. This method is quite effective but it also pertains serious issues, one of the biggest downsides is the excessive thermal cycling with high temperature delta, caused by molten metal sudden coming into contact with the relatively cold die. This heating process greatly deteriorates the die material, effectively reducing the effective lifespan of these high cost assets, increasing equipment downtime and maintenance costs, which can become a substantial cost when operating at a large scale.

This existent issue provides the opportunity for improvement in this specific stage of the HPDC process. By reducing or even eliminating this traditional method of preheating through other means that can be equally effective, long term die life can be potentially improved and lead to overall reduction of operating cost. This study looks into the possibility of utilizing an auxiliary heating device to provide the necessary heat to the die, which is a more gradual and less destructive preheating process. This alternative preheating method could prove to be an effective method in achieving the same goal of increasing die temperature.

1.9 Content Overview

- Chapter 1 provides the essential information of the research project, covering the problem statement, significance, assumptions, limitations, and delimitations.

- Chapter 2 presents and discusses relevant literature findings, providing background information on related studies and potential

- Chapter 3 reviews experimental procedures of the study, following through the steps starting with consideration on heater selection, surface heat flux requirements for the proposed heating goal, and the numerical calculations that provide estimations of heating results.

- Chapter 4 contains experiment results and analysis, along with discussions of issues encountered during the experiments, potential effects and concerns that may arise. The experimental results of the varying combinations of variables are shown and discussed.

- Chapter 5 summarizes the content of the this study, including the recommendations on continuation of research on the topic and conclusions of the current findings.

CHAPTER 2. REVIEW OF LITERATURE

2.1 High Pressure Die Casting (HPDC)

HDPC involves forcing molten metal into a die cavity under pressure, and having it solidify at a controlled rapid rate by the cooling lines running through the die. This process is ideal for mass production due to its short cycle times. But it also comes at the cost of rapid cyclic stressing of the die material, lowering its service life with the growing number of temperature cycles [6]. Data from Long's article suggests when under steady state conditions, within one casting cycle the temperature fluctuates between 240 °C and 500 °C [6]. During those cycles, if a die is stopped for brief periods, heat is lost rapidly, and the material will endure additional thermal shock when the cycle restarts. It is also determined that fluctuation magnitude and an increasing number of thermal cycles will degrade the die at a higher rate and crack formation will occur earlier and after less casting cycles [6].

For an aluminum casting plant, dies used in HPDC are crucial assets. They are also very costly to repair and replace, despite the fact that many dies utilize multiple inserts for features in dies to enable quick repair or replacement [3]. This emphasizes the importance of keeping a die in service for longer and reducing the maintenance and repairs required. Any manufacturing downtime ultimately results in significant loss of revenue [3].

By preheating the steel dies, the stress and thermal shock to a die can be reduced greatly, and this could increase the die's overall life considerably [7]. Through a series of experiments conducted in a prior study by Dadic regarding die steel wear, the effects of preheating temperatures of a specimen and impact speed with molten aluminum using a H11 hot work tool steel material was tested [7]. Labs tests conducted by Dadic indicated that preheat temperatures directly affect the wear on steel die components used in casting, and when preheat temperatures increase to over 200 °C, the wear on tested steel materials dropped significantly regardless of the impact speed with molten aluminum [7].The results of this study illustrated the benefits of preheating die material, and proving heating the die material to elevated temperatures prior to contact with molten aluminum can reduce wear significantly [7].

2.2 Die Preheating for HPDC

To the author's knowledge, there has not been any published sources that address, specifically, infrared heating of steel dies used in high pressure aluminum die casting. The closest related field would be the use of such heaters in the hot forging process, since the parts need to be heated to a specific temperature before the forging process takes place, thus it is required to have a method to heat the material [5]. In the case of forging, it is typical for the temperature requirements to be much higher than that of heating for dies used in HPDC. As their heating process is the majority heat source during manufacturing [5]. Meanwhile in HPDC, under normal operating conditions, the cycling of casting shots will provide the heat needed to maintain quasi-steady temperature for the dies.

For aluminum HPDC purposes, injection of multiple warm-up shots can be very effective in raising the dies to their operating temperature. Thus, the need for auxiliary die heating devices non-mandatory, and can be considered as an additional cost. But as production scale increases, and viewing from the long term perspective, expensive tooling and hardware repair/ maintenance expenses can escalate greatly, in which production time and cost factors to become increasingly important, under these circumstances, benefits of auxiliary heating systems may greatly outweigh their added cost and prove to be effective cost savings in the long term [4].

2.3 Infrared Radiation

Infrared radiation (IR) is electromagnetic radiation with wavelengths just above the visible light range, the visible range of light is typically considered in the wavelength region of 380 nm to 780 nm, while the infrared region lies approximately between the 800 nm to 1 mm wavelength range. Within the depicted range, IR can be subdivided into three subcategories, short wave infrared radiation (0.78 μm - 1.50 μm), medium wave infrared radiation (1.50 μm - 3.00 μm), and long wave infrared radiation (3.00 μm - 1 mm) respectively. [1]

Experiments are performed on half of a die core constructed completely of H13 hot work tool steel. Since the exact experimental data was not available for the die material's specular reflectance, optical properties have been estimated based on prior research others have conducted for similar steel material. To determine the wavelength that is more suited for heating H13 tool steel, reflectance data of AISI 304 stainless steel from Namba's 1983 publication was initially utilized as a reference [8].

Since it is desired to have the die absorb more of the radiated energy and raise its temperature quickly, having less energy reflected is a desirable trait. According to Namba, the specular reflectance on a stainless steel surface rises with both the increase in wavelength and the reduction in surface roughness. In the case of the present work, the surface roughness of the die surface is set and cannot be altered. Therefore efforts are focused on finding the optimal wavelength region that is in general most suitable for heating the material [8]. The reflectance for AISI 304 with varying surface roughness can be viewed in *Figure 2.1*, it displays the reflectance as a function of wavelength. Each curve represents a different surface roughness. In the present work, the varying levels of roughness may be representative for the varying levels of oxidation on a used die surface.

A later study by Wen in 2010 studied steel emissivity behaviors properties of H13 tool steel at elevated temperatures. The findings agree with the reflectance trends obtained for polished specimens of SS304 in Namba's paper [9]. The results can be seen in *Figure 2.2*, which shows the reflectance as a function of wavelength. The varying curves represent different material temperatures.

In conclusion, the graphs and results provided by Namba and Wen combined depict that reflectance decreases as the wavelength decreases. Thus, the IR range that is most suitable for heating H13 material lies within the SWIR bandwidth (780 nm - 1.50 μm), where reflectance is always lowest, regardless of temperature or surface roughness [8] [9].
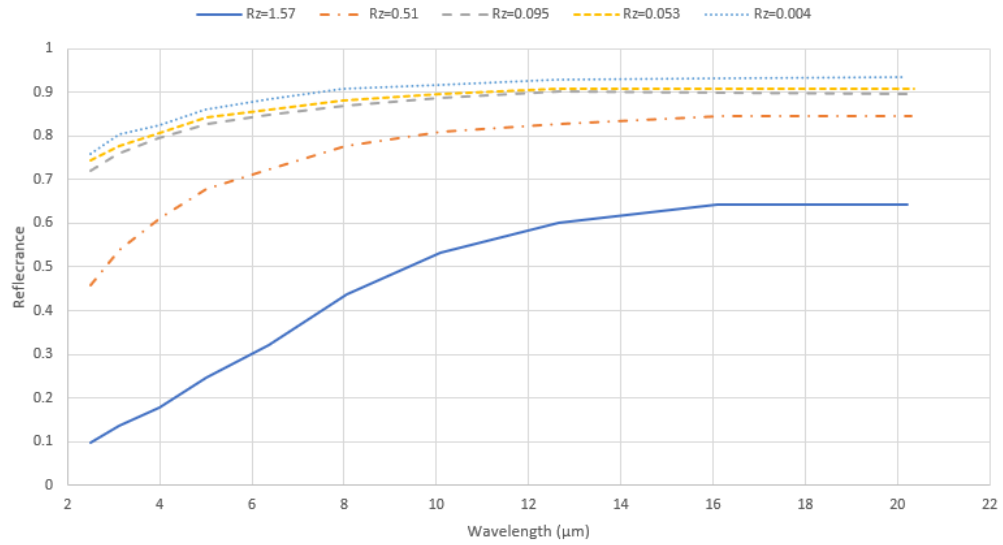
Figure 2.1. Infrared specular spectral reflectance of cold-rolled A1S1 304 stainless steel at near normal incidence as a function of surface roughness [8]
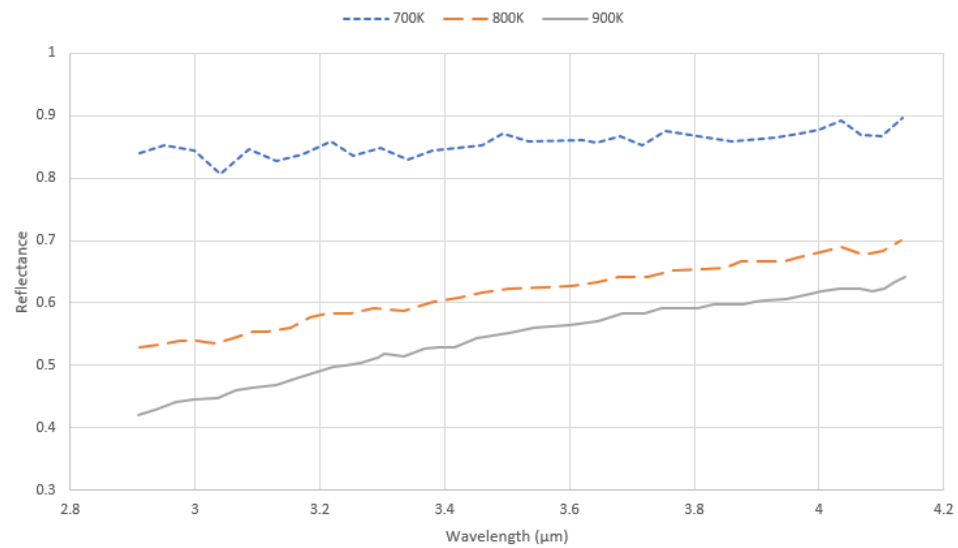
Figure 2.2. Effects of temperature on spectral reflectance for AISI H13 steel [9]

2.4 Literature Review Conclusions

High pressure aluminum die casting excels in the high volume production of aluminum components, and with the quick cycle times and large production volumes, cost become increasingly important [2]. Improving the process to become more efficient will provide huge benefits in the overall process, providing significant savings for a factory.

Dies used in the casting process need to be brought up to a certain temperature in order to produce proper castings acceptable for manufacturing purposes. With the operating temperature fluctuation between 240 °C - 500 °C, it is expected that reaching a temperature of 300 °C would be sufficient to reduce the warm up cycles required [6]. In addition, given the fact that reduced wear can be achieved by preheating die materials to temperatures above 200 °C, reaching the said 300 °C should also increase overall service life of an aluminum HPDC die [7].

To bring the temperature up to the specified target from room temperature, a heater capable of emitting radiation in the SWIR region is desired. The SWIR wavelength was chosen because the radiation is most effectively absorbed by the die material in this regime, meaning that the raising of temperature within the die should be significantly faster compared to using a heater with comparable output that operates in a longer wavelength band.

In addition, there are existing heating elements that are commercially available for purchase to construct heaters that will meet our dimension requirements. The systems are generally scalable for adaption in different die size applications. An experimental report by Blue demonstrated the feasibility of an electric short wave infrared system within a forging production environment. This study showed that the method offers the robustness needed in a production environment, and offers the ability to rapidly heat and sustain temperatures in forging billets and dies [5].

CHAPTER 3. RESEARCH METHODOLOGY

3.1 Motivation

The main benefit of preheating a die before use is to reduce the amount of warm up scrap created at the beginning of a work cycle and reduce the down time when unexpected/expected production breaks occur. The area of HPDC die heating has seldom been explored previously since it was mainly utilized in forging facilities to heat forge billets. There have been a number of publications addressing the usage of heating systems in hot forging, meanwhile, to the author's knowledge, there are no papers specifically dedicated to exploring the possibilities of infrared heating on aluminum HPDC dies. Nonetheless, the experimental study by Blue covering the use of an electric infrared heater on aluminum billets for forging also conducted additional testing on the subject of die preheating, and presented results showing the successful heating of a $12" \times 14" \times 6.5"$ die from ambient temperature to 300 $^\circ$C in less than 20 minutes, utilizing their 88 kW heater unit running at 80% power [5]. Additionally, the tests were conducted in a forging factory, proving that electrical infrared quartz tungsten halogen lamp systems have the robustness to survive manufacturing plant environments [5].

There is great potential in reducing the overall production cost for a casting plant with the use of die preheating. Currently, warm-up scrap at the beginning of production shifts account for significant waste in materials, reducing such waste would directly equate to heightened production capacity at reduced operating costs [3].

3.2 Prospeting Methods of Heating/Down-selection

The initial task was to determine a method that will be able to provide heat to the die. Based on commonly used methods in industry, we mainly considered four options: infrared, direct flame, induction, and resistance. The goal was to provide an auxiliary heating method that could function whilst the die was installed in the casting machine, and did not require the removal of the die core for off site heating.

- Infrared heating: The selected method in this study, there exists a broad variety of infrared heating devices, with options in both gas and electric powered units. The main differences lay within the operating wavelengths of the heating elements, with gas powered units mostly all in the LWIR region and used mainly in space heating. Electric units offer a broader range of wavelengths , and serve a multitude of functions [5] [10].

- Direct Flame: Typically, with direct flame heating methods, a form of burners is presented within close proximity to the material surface to be heated. The energy source is usually a combustible gas. This method can provide a high energy concentration, however it also presents potential problems such as: combustion residue depositing onto the surfaces being heated, heat concentrations at flame contacting regions, and also the extreme temperature gradients within the die due to the high heat flux the flame impinges. There is also the added difficulty in fine control of a burning open flame [11] [12].

- Induction heating: Induction is used to heat electrically conductive materials (typically steel). Typically, a coil is placed around or over the material to be heated, or it may be embedded into the part itself. Heat is generated by eddy currents flowing through the material, which cause Joule heating. This method offers fast response and rapid heating. But upfront costs to implement such systems in a production environment is typically high, due to requiring custom shaped coils matching the heated components for optimal heating performance. Moreover, maintenance is extremely difficult and costly in the case of embedded systems [11].

- Resistance Heating: This is a common heating method often seen in household electric stove-tops and electric heaters, utilizing a heating element coil heated by electrical current running through, they are robust and relatively cheap to maintain. However, they are generally more preferred in conductive or convective applications as the coil temperatures typically are lower compared to infrared heaters, producing lower intensity radiation energy at longer wavelengths [11] [13].

Among the options, direct flame did offer the highest heat flux output, and was considered alongside infrared heating as a potential candidate. However, further research in the topic also brought up the issue of possible annealing affects on the heated material. Used in the HPDC application is a H13 die, which typically has a annealing temperature around 810 - 900 °C [14] [15]. Flames which have temperatures in excess of 1000 °C pose a potential threat of destroying the die properties completely and was ultimately ruled out of consideration [16]. The chosen method in this study to heat the steel die is an electric short wave infrared heating system. Electric halogen quartz tube heating elements were selected because of: minimal startup time, SWIR wavelength band, and ease of temperature control through electrical current manipulation.

The heating element used in this heater is a cylindrical quartz tube type housing a tungsten filament. The heater prototype system was built by Infrared Heating Technologies, LLC, an industrial heating equipment supplier. Heater bulbs used in the system are manufactured by USHIO lighting company, with the specific model being QIH240-2000TS from their quartz infrared heater product lineup, which are intended for industrial heating applications. The length of each bulb is 603 mm, with a lighted length of 508 mm [17]. This type of bulb operates similarly to incandescent bulbs, using the electrical current passing through a filament to create heat. The bulbs are filled with halogen gas to extend bulb life and reliably sustain continuous high temperature operation. These halogen filled quartz bulb elements operate at a color temperature of around 2500 K, and heating is produced via radiation emitted through the halogen gas and quartz shell to the outer environment. Peak emissive wavelengths of the bulbs are in the SWIR region, which is where less energy is reflected by the die surface [8] [9] [17].

The heating performance of the electric powered halogen lamps are evaluated in this study to determine feasibility for use in heating of aluminum castings dies. The heater relies on the transfer of energy through infrared radiation. It has been determined that it is desirable to have a heater emitting short wave infrared radiation, as the surfaces are less reflective at wavelengths in the said domain (estimate determined using specular reflectance for rough SS304 surface and H13 reflectance at elevated temperatures [8] [9]). This translates into more energy being actually absorbed into the material, hence transferring the energy more efficiently and effectively.

3.3 Analytical Calculations

Calculations are done to obtain a understanding on the rough specifications of a heater suited for the task. Using analytical tools, an average heat flux required on the surface of the die to achieve the 300 °C in 30 minutes heating goal is estimated. Following, main factors that affect energy transfer are accounted for, and a heater surface average heat flux emission can be estimated. Lastly a total theoretical required output can be obtained.

Material properties will be idealized for simplification purposes. Area for heater and die will be approximated as equal, so to cover the entire die surface area. The results will be justification for the selection of the heater used in this study, describing the reason why high operating temperatures are needed for the heat source, and how surface properties will affect the heat transfer.

Wien's displacement law [13]

$$b = \lambda_{max}T = 2897.8 \quad \mu m \cdot K \tag{3.1}$$

Assuming the thermal radiation source is an ideal blackbody, Wien's displacement law indicates that the higher the temperature, the peak emissive wavelength is shorter. The heating option selected utilizes halogen filled quartz tubes with tungsten burning elements enabling a burn temperature in excess of 2400K, with peak emmisive energy at shorter wavelengths, it will allow more energy to be transferred to the steel surface.

Analytical solution for calculating slab with jump in heat flux at one boundary, and zero heat flux at other boundaries [18]
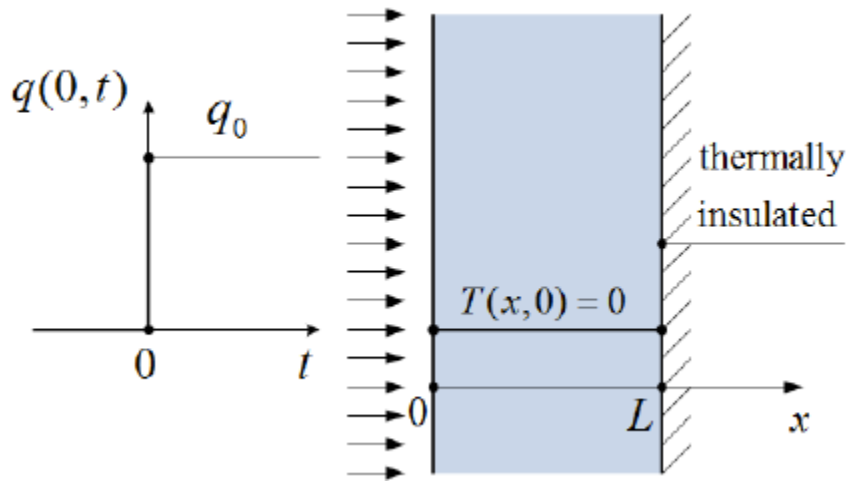
Figure 3.1. 1D transient slab schematic [18]

Given the heated slab is constructed of H13, the properties for the material are obtained as [19]. Realistically, these values may be dependent on temperature, but for calculation purposes, all values are assumed to be constant.

$\rho = 7800 \text{ kg/m}^2$

$c_p = 460 \text{ J/kg}$

$k = 24.3 \ W/m \cdot K$

$\alpha = \frac{k}{c_p \rho}$

Dimensional governing equations:

$$\frac{\partial^2 T}{\partial x^2} = \frac{1}{\alpha}\frac{\partial T}{\partial t} \quad (0 < x < L; t > 0) \tag{3.2}$$

$$-k(\frac{\partial T}{\partial x})_{x=0} = q_0 \quad (t > 0) \tag{3.3}$$

$$(\frac{\partial T}{\partial x})_{x=L} = 0 \quad (t > 0) \tag{3.4}$$

$$T(x,0) = 0 \quad (0 < x < L) \tag{3.5}$$

Dimensionless variables:

$\tilde{T} = \frac{T}{q_0 L/k}$

$\tilde{q} = \frac{q}{q_0} = -\frac{\partial \tilde{T}}{\partial \tilde{x}}$

$\tilde{x} = \frac{x}{L}$

$\tilde{t} = \frac{\alpha t}{L^2} = Fo$

Dimensionless governing equations:

$$\frac{\partial^2 \tilde{T}}{\partial \tilde{x}^2} = \frac{\partial \tilde{T}}{\partial \tilde{t}} \quad (0 < \tilde{x} < L; \quad \tilde{t} > 0) \tag{3.6}$$

$$-(\frac{\partial \tilde{T}}{\partial \tilde{x}})_{\tilde{x}=0} = 1 \quad (\tilde{t} > 0) \tag{3.7}$$

$$(\frac{\partial \tilde{T}}{\partial \tilde{x}})_{\tilde{x}=1} = 0 \quad (\tilde{t} > 0) \tag{3.8}$$

$$\tilde{T}(\tilde{x},0) = 0 \quad (0 < \tilde{x} < L) \tag{3.9}$$

The solution is an exact analytical solution for heat conduction, variables for the provided function are the dimensionless location $\tilde{x}$, time $\tilde{t}$, and the accuracy desired A, which determines a computational accuracy of 10^{-A}. The resulting outputs are $\tilde{T}$ and $\tilde{q}$, which in this case only $\tilde{T}$ is used and converted to dimensional temperature values for viewing.

For $0 \leq \tilde{x} \leq 1$

$$\tilde{T}(\tilde{x},\tilde{t}) \approx \begin{cases} 2\sqrt{\tilde{t}} \ \mathrm{ierfc}\left(\frac{\tilde{x}}{2\sqrt{\tilde{t}}}\right) + 2\sqrt{\tilde{t}} \ \mathrm{ierfc}\left(\frac{2-\tilde{x}}{2\sqrt{\tilde{t}}}\right) & \text{for } 0 \leq \tilde{t} \leq 0.15 \\ \begin{aligned} (\tilde{t}+\frac{\tilde{x}^2}{2}-\tilde{x}+\frac{1}{3}) &- 2\frac{\cos(\pi\tilde{x})}{\pi^2}\exp(-\pi^2\tilde{t}) \\ &- \frac{\cos(2\pi\tilde{x})}{2\pi^2}\exp(-4\pi^2\tilde{t}) \end{aligned} & \text{for } \tilde{t} > 0.15 \end{cases} \qquad (3.10)$$

Die dimensions are approximated to be 20" × 20" × 4", thus the heated slab is determined with $L = 4$". For the 1D simulation, a starting temperature of 27 °C (300.15 K) was assumed, and a total time of 1800 seconds (30 minutes) was evaluated using an accuracy of A = 15. Utilizing the dimensionless temperature and heat flux solutions provided in Filippo de Monte's and James V. Beck's article assuming all boundaries are perfectly insulated [18]. The calculation results show the surface heat flux on a 4" thick slab would need to be at 43.2 kW/m^2 to meet the requirement of achieving 300 °C surface temperature in 30 minutes.

The graph illustrated in *Figure 3.2* displays the analytical transient solution for the 1D slab with a thickness of 4". The temperature is taken at $x = 0$", which gives $\tilde{x} = 0$. The return solution $\tilde{T}$ values are reverted into dimensional T values in °C and plotted as a function of time, which is converted from seconds to minutes.
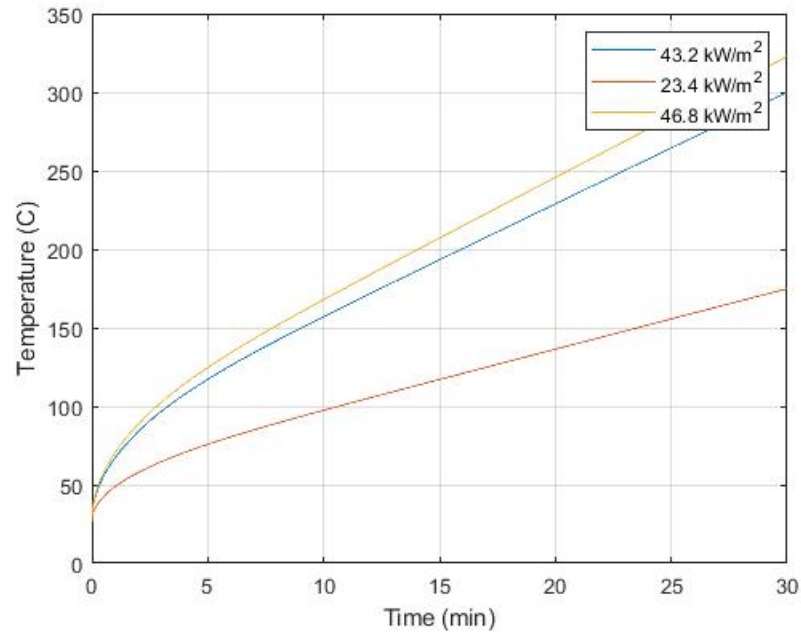
Figure 3.2. 1D slab analytical solution for 43.2 kW/m^2, 23.4 kW/m^2 and 46.8 kW/m^2 surface heat flux at $x = 0$, curves show temperature as a function of time

Based on the initial heating goal, combined with the knowledge from Long's paper, a target window was proposed. The target threshold was determined to be at approximately 240 °C, which is the low temperature point of the die during a typical casting cycle [6]. Furthermore, assuming the goal of the heating system is to assist in the preheating process and not increase the temperature to high temperatures, a target window of achieving 200 °C - 300 °C within the time frame of 30 minutes was chosen. Nonetheless, the overall experiment end target would remain to be achieving the target of 300 °C beginning from ambient for ease of testing data range and consistency purposes.

View factor for aligned parallel rectangles

The view factor is the fraction of the radiation leaving surface *i* that strikes surface *j* directly [13].
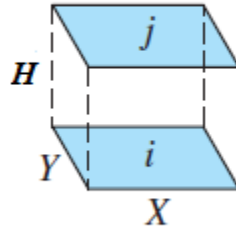
Figure 3.3. Aligned parallel rectangles [13]

$\overline{X} = X/H$ and $\overline{Y} = Y/H$

$$F_{i \to j} = \frac{2}{\pi \overline{X}\overline{Y}} \left\{ \ln \left[\frac{(1+\overline{X}^2)(1+\overline{Y}^2)}{1+\overline{X}^2+\overline{Y}^2} \right]^{1/2} + \overline{X}(1+\overline{Y}^2)^{1/2} \tan^{-1} \frac{\overline{X}}{(1+\overline{Y}^2)^{1/2}} \right.$$
$$\left. + \overline{Y}(1+\overline{Y}^2)^{1/2} \tan^{-1} \frac{\overline{Y}}{(1+\overline{Y}^2)^{1/2}} - \overline{X} \tan^{-1} \overline{X} - \overline{Y} \tan^{-1} \overline{Y} \right\} \qquad (3.11)$$

The heating surface and heated die surface can be assumed equal in size, as both surfaces are approximately a 20" × 20" area. thus a view factor can be calculated based on the view factor equation for aligned parallel rectangles. Where $L = 4.6", X = Y = 20"$, thus

$\overline{X} = \overline{Y} = 4.3478$

Calculating equation 3.10 using these values for $\overline{X}$ and $\overline{Y}$, a view factor is obtained for a standoff distance of 4.6". This is the minimum distance limited by die feature protrusions and the heater protection mesh.

$F_{heater \to die} = F_{i \to j} = 0.67 \quad @H = 4.6"$

Figure 3.4 presents the view factor as a function of standoff distance for aligned parallel rectangles with an area of 20"×20".
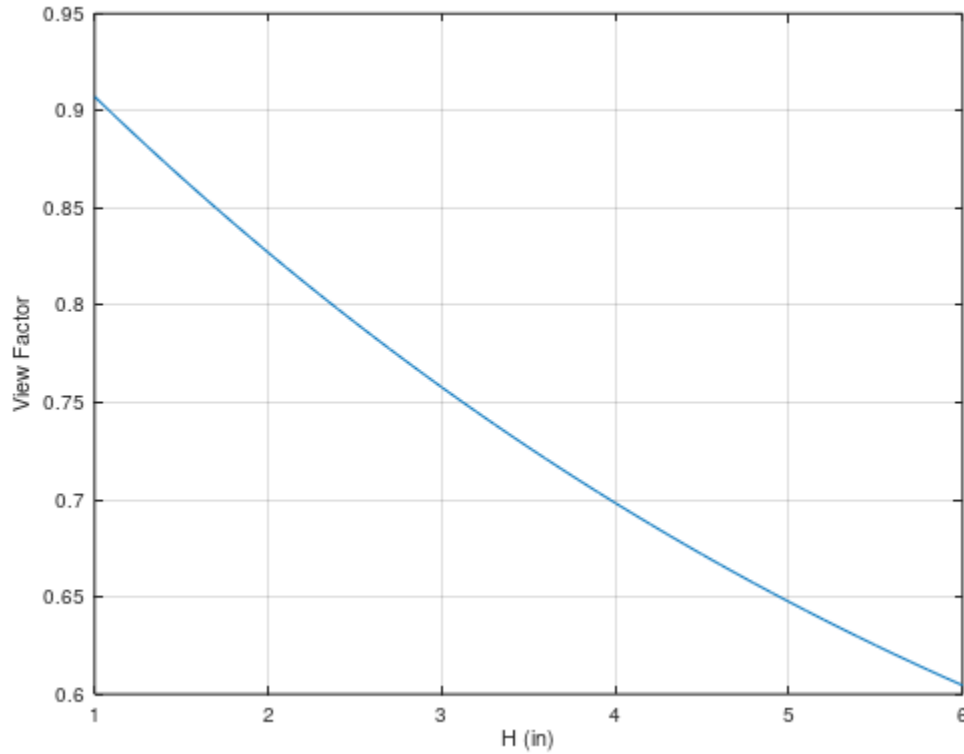
Figure 3.4. View factors relative to varying standoff distances from die surface

Knowing the required surface heat flux, an estimate of the heating area average heat flux can be calculated.

$$q_{unidirectional} = q_i = \frac{q_j}{F_{i \to j}} = \frac{43.2 kW/m^2}{0.67} = 64.5 \quad kW/m^2$$

Where q_i is radiating surface heat flux, and q_j is the estimated surface heat flux of 43.2 kW/m^2 from the 1D analysis.

Combining the view factor of the experimental setup and the calculated required surface heat flux of $43.2 \; kW/m^2$. A heating surface with an area of 20" × 20" will need to be outputting an average heat flux of 64.5 kW/m^2 at a distance of 4.6", in order to achieve the goal of heating the surface of the die slab to 300 °C in 30 minutes time. *Figure 3.4* shows the view factor as a function of standoff distance H.

$$P_{bidirectional} = 36 \quad kW$$

$$A = X \times Y = 0.508 \times 0.508 = 0.258 \quad m^2$$

$$q_{bidirectional} = \frac{P_{bidirectional}}{A} = \frac{36}{0.258} \frac{kW}{m^2} = 139.5 \quad kW/m^2$$

$$q_{unidirectional} = \frac{q_{bidirectional}}{2} = 69.8 \quad kW/m^2$$

The selected heater unit has a approximate heating area of 20" × 20", and with a total maximum output of 36 kW emitting radiation on two sides, it would produce a theoretical average surface heat flux of 69.8 kW/m^2, satisfying the initial 65.6 kW/m^2 heat flux goal.

However, the reflectance factor must also be taken into account when considering the actual energy transferred to the die surface. The die specimen used in this study is a retired component that has been heavily used in HPDC production. Through visual inspection, the surface consists of multiple areas with varying degrees of roughness and coloration. As an initial conservative estimate, it will be assumed that the whole surface has a uniform reflectance of 0.5. Using it as a general assumption of the average reflectance of the entire surface, which consists of varying coloration and roughness, this is most likely higher than the actual value.

$$q_{surf,est} = \rho_r \times F_{heater \rightarrow die} \times q_{unidirectional}$$

$$= 0.5 \times 0.67 \times 69.8 \text{ kW/m}^2 = 23.4 \quad kW/m^2$$

After considering the reflectance factor, the estimated final surface heat flux on the die would become 23.4 kW/m^2, a much lower value than the calculated 43.2 kW/m^2 required, the resulting heating curve is also shown in *Figure 3.2*.

Additionally, under real world conditions, further losses are to be expected. In the analytical solution, it is assumed that all boundaries are perfectly insulated, meanwhile in actual experimentation, the die will most definitely experience convective and conductive losses to its surroundings. A flat mirror reflector is to be used to convert the bidirectional heater into a unidirectional unit. Doing so would increase the maximum heat flux output, and provide higher heating rates. The heater unit would also be considered to be moved closer to the die surface after the removal of the protective mesh. These alterations would both improve the heating performance and potentially compensate for the losses mentioned above, and possibly further reduce the time required to reach 300 °C. The resulting gains are to be quantified and compared with the bidirectional setup.*Figure 3.2* also provides a curve showing a surface heat flux of 46.8 kW/m^2, which uses a quick estimation assuming the flat reflector will simply double the output.

<div align="center">3.4 Experiment Method</div>

<div align="center">3.4.1 Heater design</div>

An IR heating unit that operates in the SWIR region is used; the equipment is custom built to provide a maximum power output of 36 kW with power varying ability provided from a 4-20mA signal input. Heat is generated by 18 quartz halogen bulbs outputting 2 kW each, they are positioned parallel to each other and spaced $1\frac{1}{16}$" apart, providing a heating area of 20"x19-1/8" as illustrated in *Figure 3.5*. The heating unit is mounted to an 80/20 aluminum frame that is custom built with the sole purpose of holding the heater, and is capable of position adjustment in the vertical, horizontal planes. Standoff distance from die surface is set by the height adjustment of the horizontal beams supporting the heater, which can be altered freely across the length of the frame's vertical beams.
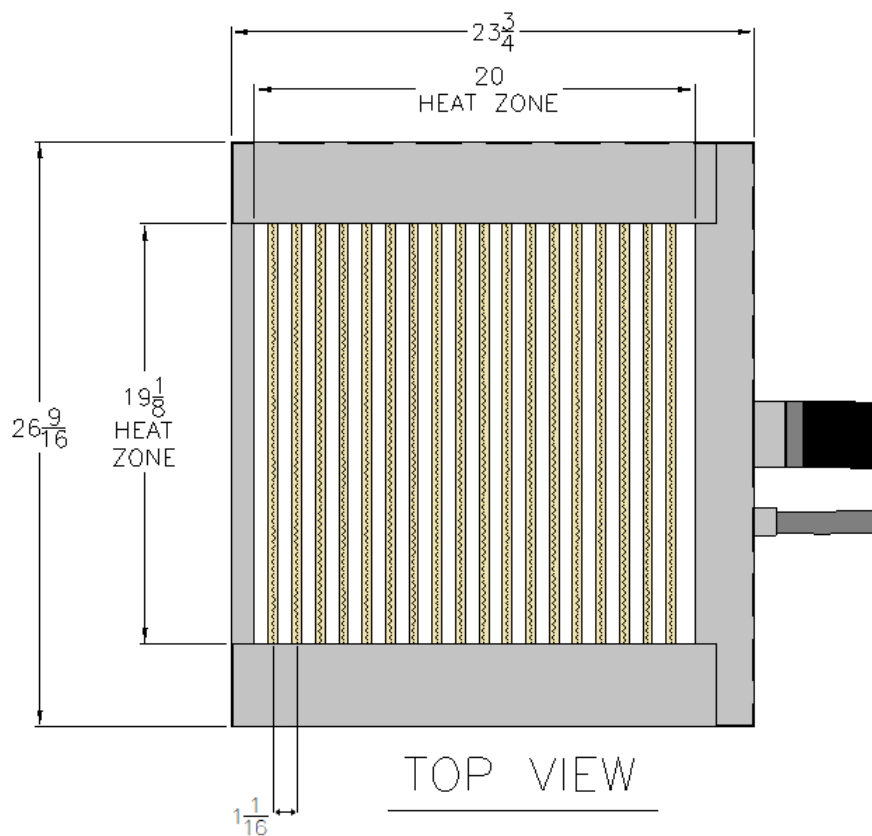
Figure 3.5. Drawing of heater unit

3.4.2 HPDC die specimen
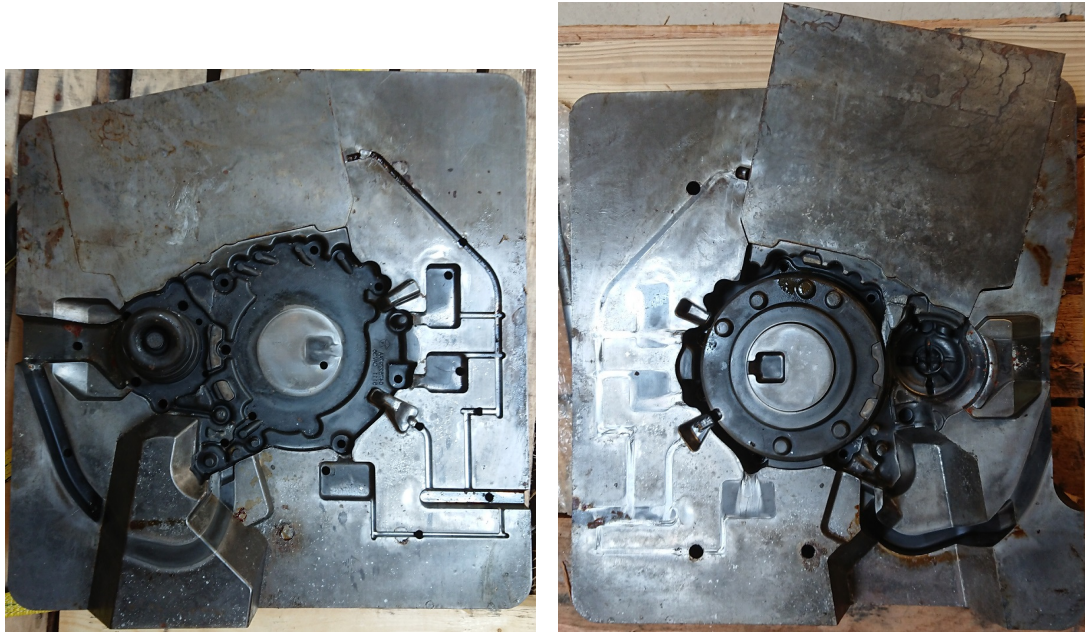
Figure 3.6. Die core top (L) and bottom (R) halves, the top was used in this study to conduct preheating tests.

The die core specimen as shown in *Figure 3.6* is used for testing. The die is in the casting of the Chrysler 948TE transmission intermediate plate, and is provided by FCA's Kokomo casting plant. The die consists of two halves that mate together and multiple inserts that complete the die cavity. The material of the components is H13 tool steel. Used in this study is the smaller upper halve of the die core, as it is deemed to have sufficient features to provide a good representation of a die surface. Also, this half can be handled more safely due to it being a lighter component overall. The die components have clearly been heavily used, as significant wear can be observed easily.

3.5 Experiment Apparatus Components

Listed here is an overview and detailed explanation of the equipment/apparatus used in the research, categorized as heater assembly, heater mount, and heater enclosure,

3.5.1 Heater

The complete heater assembly consists of the heating unit, control panel and blower. The heater design is shown as in *Figure 3.5*, it offers a maximum output of 36 kW, with possible partial power operation between 0-100 percent.By design it provides bi-directional heating capability, with the heating elements exposed on either side of the heater frame.

The heating elements of the heater are 18 individual 2kW tungsten halogen quartz tube bulbs, they emit the short wave IR radiation that is needed to heat the die. Cooling of the terminals is required to prevent overheating, and is provided by a blower pushing air through cooling ducts on either side of the heater. Cool air is blown through a single inlet on one end of the frame, where it diverges into two passageways on either side (exposed passageway and bulb terminals can be seen in *Figure 3.7*), and finally hot air is exhausted through the opposing end through two outlets.

The elements are protected by a stainless steel mesh bolted on both faces of the heater, in which it also limits the closeness that the heater can be positioned to the die surface if not removed, also shown in *Figure 3.7*.

Figure 3.7. Partially assembled heater frame with a better view of protective mesh and exposed terminal ends

3.5.2 Heater mount

The heater assembly is mounted to a solid 1.5 inch 80/20 aluminum frame, which can be viewed in *Figure 3.8*, the frame is secured onto a vibration dampening table via bolts. It has been constructed to provide the necessary freedom of movement required for the experiment. The mounting device permits free adjustment of the heater position along the vertical and horizontal axis within the dimensional limits of the frame.
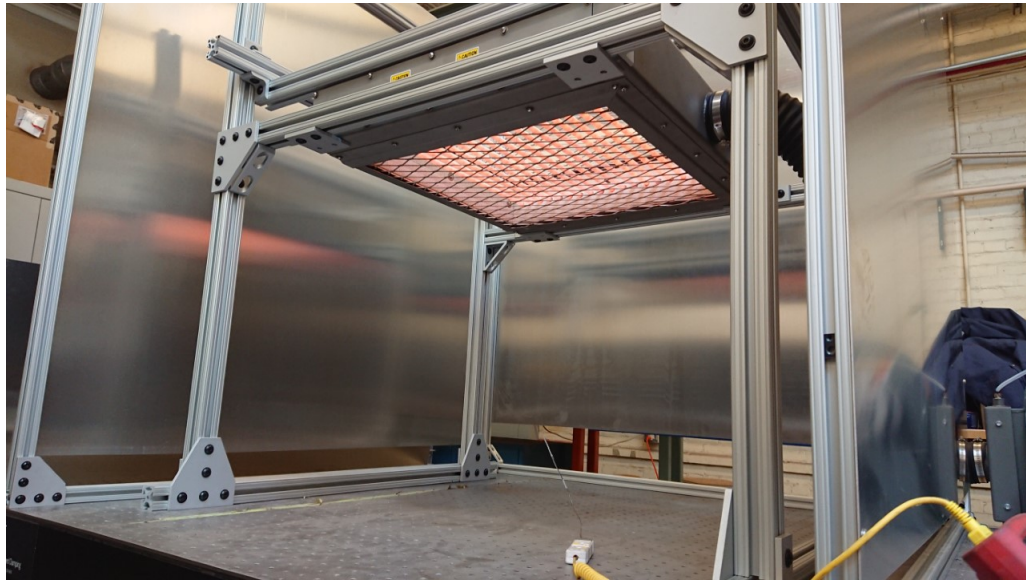
Figure 3.8. Heater on mount running at a low power setting

3.5.3 Insulation

An aluminum foil covered ceramic fibre soft insulation material was used to protect the optical table used to support the experiment setup, it was also used to insulate the sides that are not directly facing the heating elements to evaluates the effectiveness of limiting convective and losses. The insulation setup is shown in *Figure 3.9*.
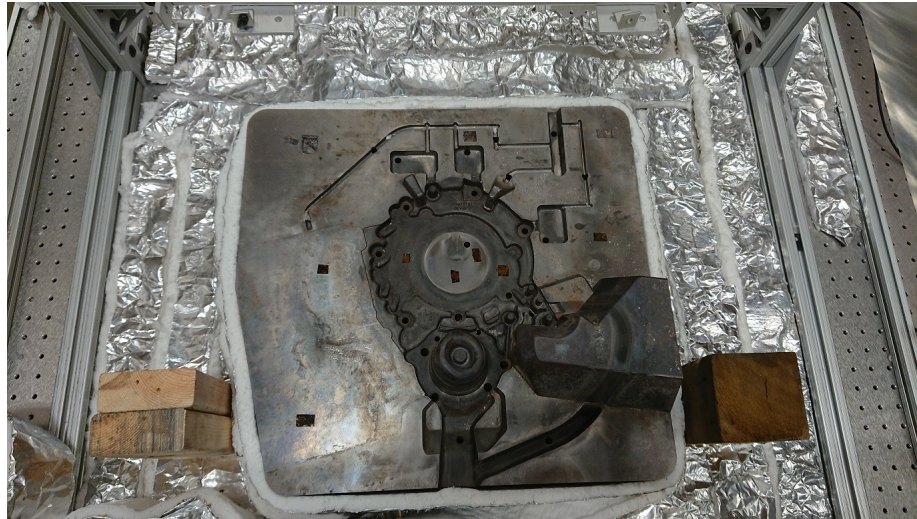
Figure 3.9. Insulation used to wrap die and isolate table surface

3.5.4 Top reflector

A flat reflector modification was tested to output a higher heat flux for heightened heating performance. A SS304 mirror reflector was used, as shown in *Figure 3.10*, the intent is to evaluate the performance gains such a device would bring for heating the die surface. The reflector presents a polished mirror finish facing the heating elements to reflect the radiation, and the backside is painted black with high temperature resistant paint to increase emissivity. The reflector dimensions are 24" X 24" in width and length, and 0.03" in thickness.
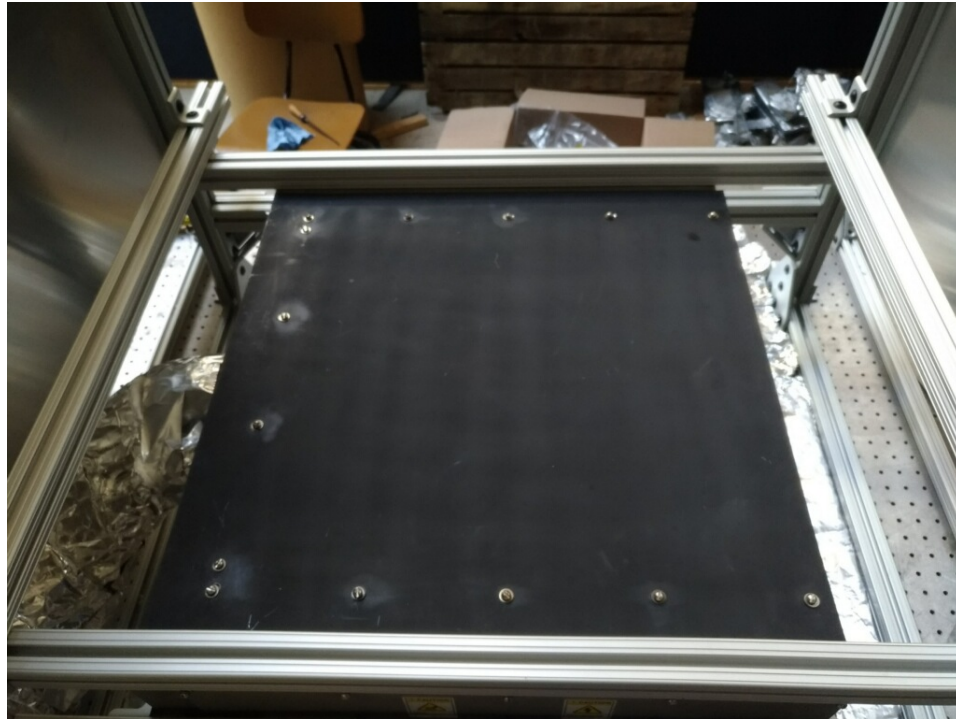
Figure 3.10. Reflector installed covering the heater top surface, viewed from the top showing the painted side opposing the polished reflective side

3.5.5 Side reflectors

Two flat SS304 mirror reflectors of identical material to the top reflector are bolted to either side of the heater for testing of its effects on heating performance, the intent is to see whether having reflectors on the sides will redirect radiation that may otherwise be lost and improve the heating performance. The material is identical to the top reflector and is bent to fit around the die and bolt under the heater. one reflector is shown in *Figure 3.11*, a simple schematic of the final reflector setup viewed from the side is shown in *Figure 3.12*.

Figure 3.11. Side reflector
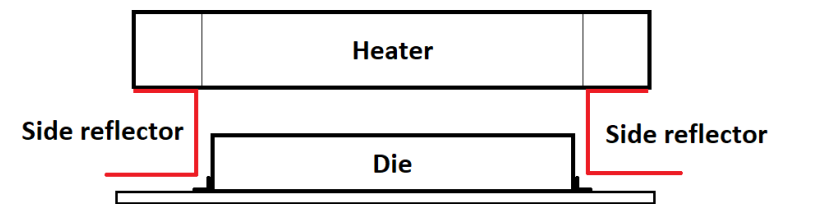
Figure 3.12. Side reflector schematic

3.5.6 Control panel

The control panel as seen in *Figure 3.13* provides the basic control of the heater system with on/off buttons for the blower and heater independently. Control of the actual heater power output has been modified to take a 4-20mA signal from the Labview software via a National Instruments DAQ unit. The signal connector has been wired to current transducers under the power supply cables to monitor the current draw of the entire unit. The E-stop and breaker are both capable in cutting power to the entire unit if needed.

Figure 3.13. Control panel for heater system

3.5.7 Blower

The blower shown in *Figure 3.14* utilizes a simple flexible hose to pump air into the heater outer housing to provide the cooling for the bulb terminals, it is also connected and controlled via the control box with a simple on/off function.
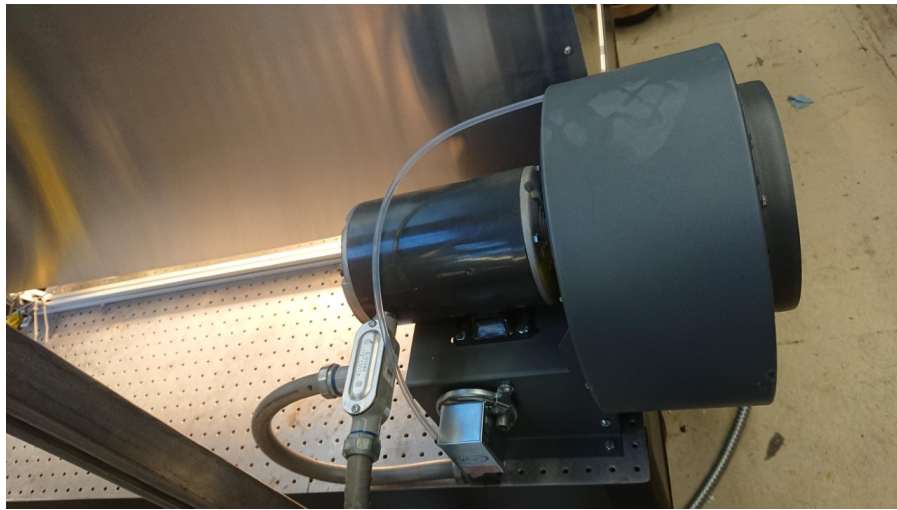
Figure 3.14. Blower feeding a duct routed through the heater frame to provide cooling for heating element terminals

3.5.8 Die Support Rails and Guides

The die is placed on top of by 1 inch 80/20 framing with UHMW Plastic wear strips underneath to provide clearance for thermocouple wiring, they also serve the purpose to provide some insulation between the die and table to reduce conduction losses, as shown in *Figure 3.15*(L).

3.5.9 Heater enclosure and shielding

The entire heating assembly is shielded using aluminum sheet panels fastened to an outer frame surrounding the heater and die, its function is to block the short IR radiation and heat produced by the heating elements, so that surrounding personnel is not exposed directly. The heater thermal radiation shielding is also constructed using 80/20 aluminum framing, with 1 inch bar stocks and 0.04" thick aluminum panels covering all four sides of the enclosure. Bottom is spaced and top is open to allow for air circulation, which is visible in both *Figure 3.15*(L) and *Figure 3.15*(R).

Figure 3.15. (L)Heater mount and (R)shielding enclosure

3.5.10 Assembly overview

The assembled heater system is shown in *Figure 3.16*, prior to the control box and power cable installation. *Figure 3.17* shows the simplified schematic of the heater system.
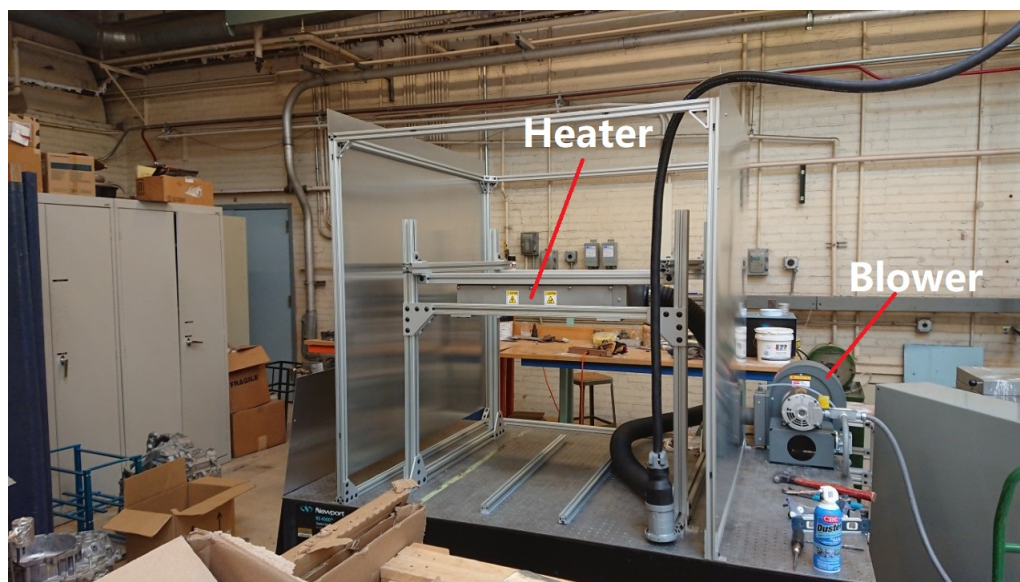
Figure 3.16. Heater secured on mount before die placement
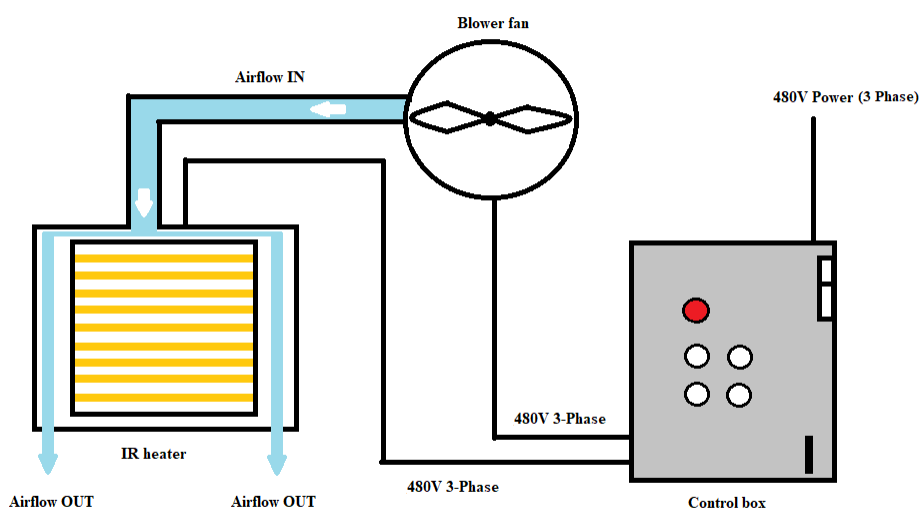
Figure 3.17. Heater system schematic

3.6 Temperature Sensor Positioning

Temperature readings were acquired using K-type stainless steel sheathed thermocouples, they were embedded into the die entering from the backside opposing the die surface, where they are positioned strategically in various locations of interest across the die. Locations were chosen based on die geometry, surface levels, and pronounced features that were expected to affect heating. Holes were drilled in precisely from the backside of the die using a solid carbide drill bit attached to a Hurco 3-axis CNC mill. Distance from the surface is set to be 1-1.5 inches so that temperature gradient within the die material can be obtained, closer distances were considered but soon rejected due to drill bit limitations and consumption. Hole positioning on die is shown in *Figure 3.18*, with Table 3.1 indicating the a precise measurements of the location and depth of the holes.
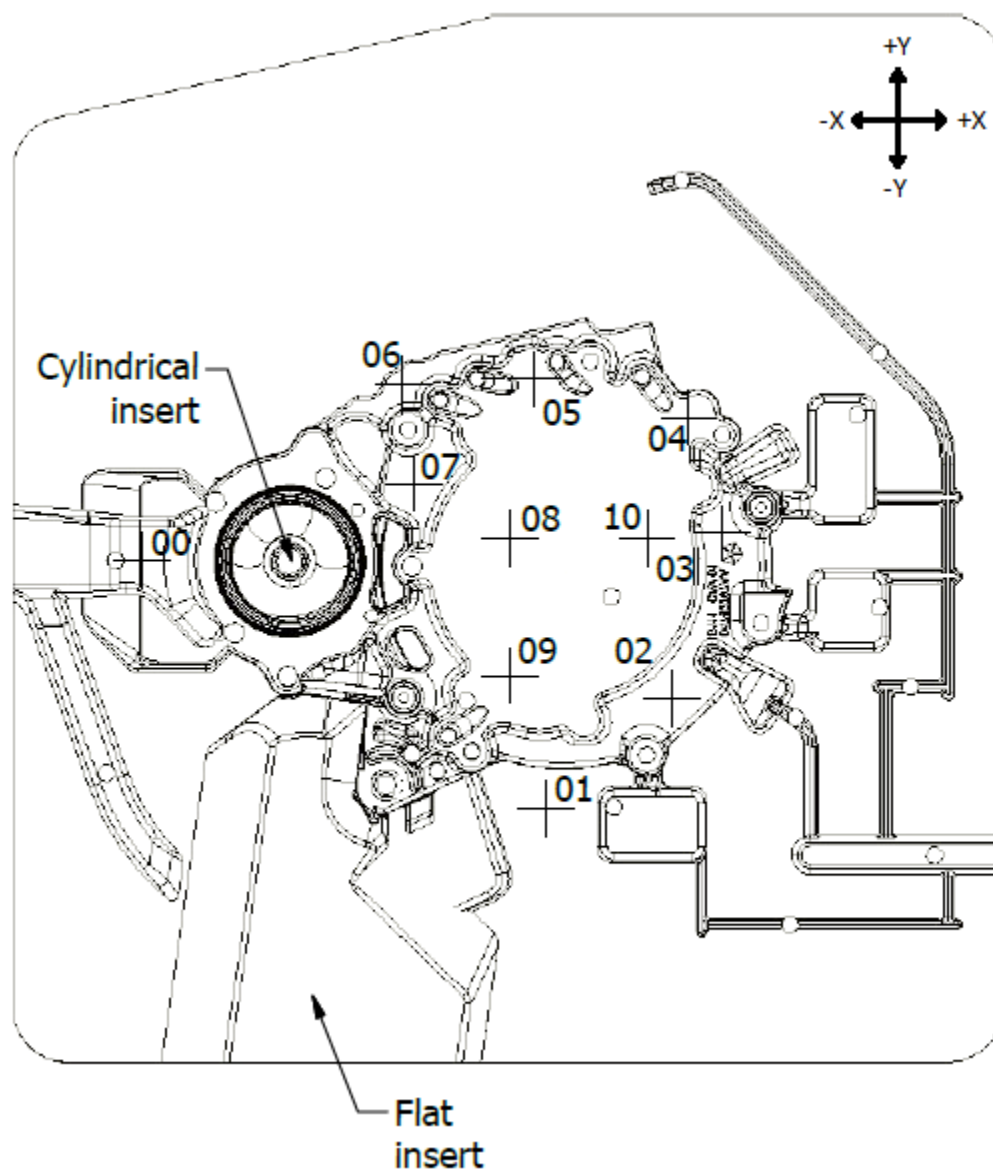
Figure 3.18. Temperature measurement positions (View Table 3.1 for precise positioning).

Table 3.1. Precise location and depth of holes used for thermocouple installation.

Hole	X	Y	Drill Depth	Distance from heated surface
00	-6.689	0.412	1.906	1.00
01	0.661	-4.912	3.00	1.00
02	2.961	-2.912	2.624	1.00
03	3.861	0.088	2.624	1.00
04	3.261	2.188	2.406	1.00
05	0.461	2.888	2.406	1.00
06	-1.939	2.788	2.941	1.00
07	-1.739	0.988	2.624	1.00
08	0	0	2.406	1.00
09	0	-2.5	1.906	1.50
10	2.5	0	1.906	1.50

Table 3.1 notes:

Values are measured in inches.

Position X/Y coordinates are all relative to T08 which is used as the origin.

Position T08 is the geometric center of the die.

Holes are drilled from backside of die towards the heated surface.

Drill bit specifics:

Brand: Guhring   Model: Series 6511

Flutes: 2   Material: Solid carbide

Diameter: 9/64"   Point angle: 135°

Flute Length: 96mm   Overall length (OAL): 136mm

Shank Diameter: 6mm   Cooling: None

Thermocouples were secured with the assistance of JB weld at the surface of the insertion holes. The completed installation prior to moving the die onto the experiment table is shown in *Figure 3.19*.

Figure 3.19. Thermocouples installed into the back of the intermediate plate die

3.7 Data Acquisition and Control

Data acquisition and heater control is done using LabView software as shown in *Figure 3.20*, connection between the PC and data acquisition devices is done with three National Instrument CompactDAQ I/O Modules mounted in a single chassis, as shown in *Figure 3.21*. The functions are to output a 4-20 mA control signal to the heater control box for altering heater power levels, receive thermocouple temperature readings from the 13 different locations within and outside the die, and lastly return current readings from the three power cables of the 3-phase system obtained through three AcuAMP ACT050-42L-S Current Sensing Transducers outputting a 4-20 mA signal set to correspond to values between 0-50 A.
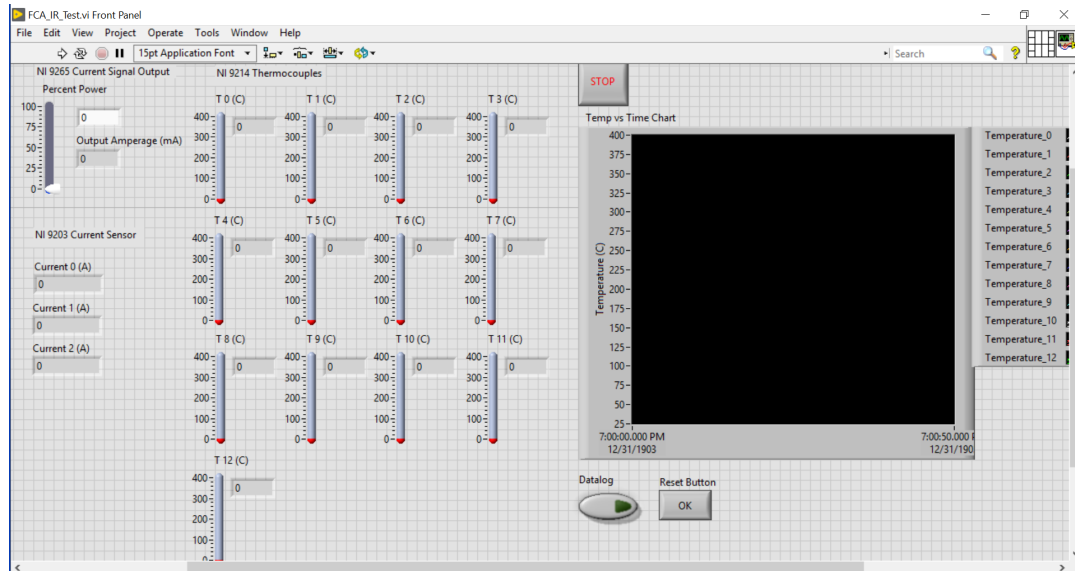
Figure 3.20. Simple Labview virtual interface for heater power control, monitoring of temperatures and current readings, and data logging. T 11 and T 12 correspond to enclosure and ambient temperature respectively.

Figure 3.21. From left to right: National Instruments NI-9265 (current output module), NI-9203 (current input module), NI-9229 (voltage input module, not used), NI-9214 (temperature input module)

Specifically, the DAQ modules used are:

- NI-9265: current output module, providing the 4-20mA signal for power heater control.

- NI-9203: current input module, receiving the signals from current measuring devices.

- NI-9214: thermocouple signal receiving module for temperature measuring.

All signals are sent and received through LabView software on a computer connected to the DAQ cards. All tasks are performed through a single Virtual Instrument (VI) shown in *Figure 3.20*. Temperature measurements are recorded at a rate of 1Hz, and saved to a data file for later analysis.

3.8 Experiment Method

For the experiment, heating performance is evaluated by the time needed for the die surface to achieved a set temperature delta from the starting temperature. From the findings based on prior literature and calculated results, the given heater design alone is not able to achieve the set target temperature within the proposed time frame, and thus a selection of four assisting variables are used to aid in achieving the target, they are each evaluated to determine their effectiveness in increasing heating performance. Due to the variation in ambient temperatures throughout the experiment period, the starting temperature of the die prior to heating is not constant. The variation in starting temperatures resulted in a possible variations in the heating time when running repeat experiments. Thus, in order to have a more direct comparison of the heating performance, the time required for the die to gain a temperature delta of 260 °C is to be used for analysis purposes. Repeated experiments were run for significantly outlying results to ensure consistency and credibility.

3.8.1 Experiment Procedure

A standard operating procedure of the experiment setup was created to ensure safe and consistent operation, the following section will provide a simple overview of the procedure.

1. Heater is positioned and centered above intermediate plate die that is laying horizontally on table with die surface facing up.

2. Heater is placed at the desired standoff distance relative to the upper surface of die.

3. Heater is turned to full power using a 0-100 percent based control that translates to the corresponding current signal.

4. Time elapsed, temperature and current readings are monitored real time by the operator and recorded automatically.

5. Once target temperature is reached at the reference position, heater is turned off manually.

6. Blower is turned after a given cool down period to prevent possible damage to the equipment from heat soak.

7. All data recorded is exported and sorted for later analysis.

Additional notes:

- Airflow from cooling does not directly impact the die during the experiments process, but may provide accelerated circulation of air within the enclosure, which is consistent in all experiments.

3.9 Shake Down Testing

A test run was first conducted under low power as shown in *Figure 3.22*, followed with additional runs with incremental increases in power level. The runs were done to ensure the safe and proper functionality of the equipment and data acquisition devices.
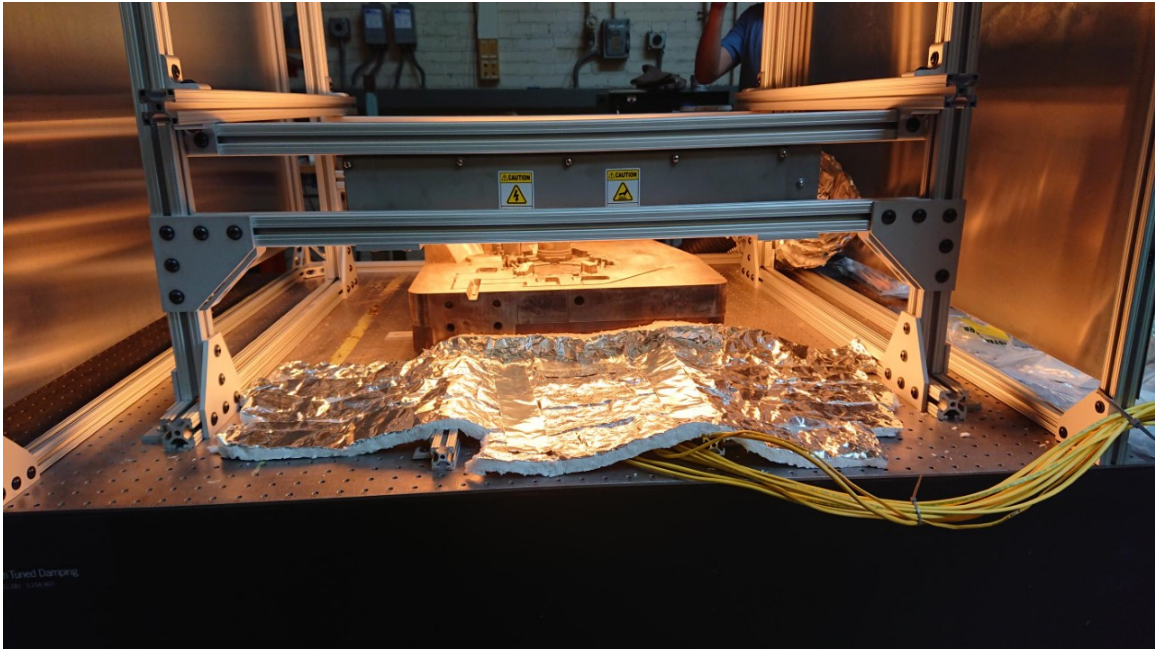
Figure 3.22. Die aligned under the heater conducting initial test run on 30% low power

The multitude of tests demonstrated the heater could be operated safely and functioned properly. All thermocouples returned proper temperature readings, and power level could be adjusted accordingly. Heater system mounts were stable and secure, meanwhile the aluminum panel enclosure provided adequate protection for surrounding personnel from thermal radiation and bright light emitted by the heater. Heater power was tested starting at 10%, and then gradually raised in increments of +10% up to 80%, with each power setting left running for brief periods of around 5 - 15 seconds. A final test run was done at 100% full heater capacity until the die reached 300 °C. Temperature readings within the die all raised steadily while ambient temperatures stayed relatively stable during the test runs. In conclusion, the shakedown tests were successful, and they were sufficient to prove that the prototype die heating system was ready for actual experimentation.

3.10 Design of Experiment

To quantify the effects of different heater configurations and heat augmentation devices (i.e. reflectors), a full factorial test was performed, followed with a two-sample t-test to analyze to results. The heating time was used as the quantifiable result. Given two levels for each factor, the test matrix includes every possible combination of factors. Factors considered were:

1. A high(4.6") and low(3.6") standoff distance.

2. With and without insulation material around the die.

3. With and without flat mirror reflectors on heater to redirect radiation towards the die surface.

4. With and without side reflectors to redirect the radiation around the sides of the die.

It should be noted that the heater was run at full power in every experiment. In total, 16 experiments were conducted. The list of experiments is shown in Table 3.2 which also list variable combinations for each experiment.

Note: **Y: Yes, variable is utilized; N: No, variable is not utilized**

Table 3.2. List of Experiments

Test #	Standoff Distance (in)	Insulation	Reflector (Top)	Reflector (Side)
01	4.6	N	N	N
02	4.6	N	N	Y
03	4.6	N	Y	N
04	4.6	N	Y	Y
05	4.6	Y	Y	Y
06	4.6	Y	N	Y
07	4.6	Y	Y	N
08	4.6	Y	N	N
09	3.6	N	N	N
10	3.6	N	N	Y
11	3.6	N	Y	N
12	3.6	N	Y	Y
13	3.6	Y	Y	Y
14	3.6	Y	N	Y
15	3.6	Y	Y	N
16	3.6	Y	N	N

CHAPTER 4. RESULTS

Initial test runs had higher heating times compared to final results, the times would significantly reduce with each heating and cool-down cycle. All results used in later analysis were obtained after the test setup conducted under identical circumstances could produce consistent results.

Experiments were all conducted under ambient conditions, where the ambient temperature was not controlled. All thermocouple probe temperatures were monitored and recorded, including 11 locations within the die and 2 external probes measuring ambient temperatures inside and outside the heating enclosure. Real time current draw by the heater was monitored as well. The heating system was set to run at full power throughout the duration of the experiments, meanwhile all probe temperatures were measured and recorded until the end of the experiment, which is indicated by the thermocouple at location #8 (T08) reaching 300 degrees Celsius. The reason this location was chosen was due to it being the geometric center of the die, considering the variation of height and features across the die surface, the central location is a relatively flat surface that is not too pronounced nor recessed.

4.1 Experiment Results

Table 4.1 is the brief overview of the result data corresponding to the experiment number #, showing the starting temperature of each experiment, and the time required for T08 to increase by a temperature delta of 260 degrees Celsius. The fastest heating time achieved was 19.87 minutes in experiment #13 which used a 3.6 inch standoff distance, insulation, top reflector, and side reflector. The slowest heating time was 53.40 minutes in experiment #01 which used a 4.6 inch standoff distance, no insulation, no top reflector, and no side reflector.

Table 4.1. List of Experiments results (Refer to Table 3.2 for specifics)

Exp #	Start Temp (°C)	+Δ260°C Time (min)
01	21.28	53.40
02	25.12	49.88
03	23.05	25.07
04	26.44	23.15
05	25.41	21.45
06	25.74	47.88
07	22.92	24.60
08	21.03	49.77
09	22.02	42.50
10	21.68	43.25
11	21.91	20.80
12	21.73	20.17
13	23.84	19.87
14	21.21	42.65
15	27.85	21.35
16	26.69	43.85

<u>4.2 Comparing results</u>

Heating curves at the geometric center of the die (TC 08) have been grouped into pairs, consistent with the two-sample t-test, and graphed for visualized comparison of the effect of each factor tested.

4.2.1 Varying standoff distance

Two experiments having standoff distances of 4.6" (experiment #01) and 3.6" (experiment #09) were compared, as shown in *Figure 4.1*. In both cases,

- Insulation (N)

- Top reflector (N)

- Side reflectors (N)

The heating curve was steeper for experiment #09, and the heating time was 42.50 minutes compared with the heating time of 53.40 minutes for experiment #01. This shows that the closer standoff distance resulted in faster heating time.
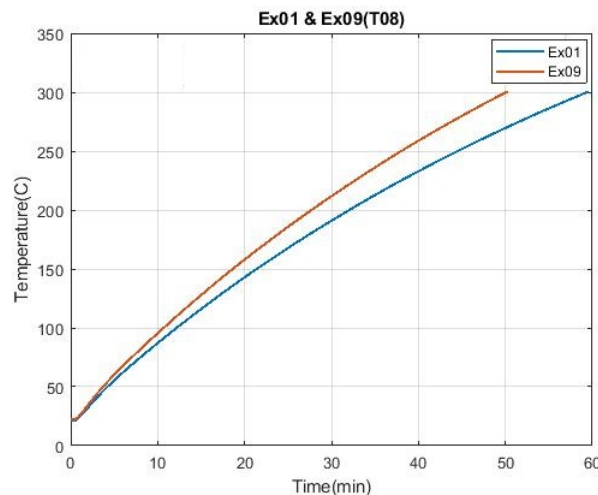
Figure 4.1. Experiment #01 and Experiment #09 T08 Heating Curves.
Standoff distance was 4.6" in #01 and 3.6" in #09.

Two experiments having standoff distances of 4.6" (experiment #02) and 3.6" (experiment #10) were compared, as shown in *Figure 4.2*. In both cases,

- Insulation (N)

- Top reflector (N)

- Side reflectors (Y)

The heating curve was steeper for experiment #10, and the heating time was 43.25 minutes compared with the heating time of 49.88 minutes for experiment #02. This shows that the closer standoff distance resulted in faster heating time.

Figure 4.2. Experiment #02 and Experiment #10 T08 Heating Curves.
Standoff distance was 4.6" in #02 and 3.6" in #10.

Two experiments having standoff distances of 4.6" (experiment #03) and 3.6" (experiment #11) were compared, as shown in *Figure 4.3*. In both cases,

- Insulation (N)

- Top reflector (Y)

- Side reflectors (N)

The heating curve was steeper for experiment #11, and the heating time was 20.8 minutes compared with the heating time of 25.07 minutes for experiment #03. This shows that the closer standoff distance resulted in faster heating time.

Figure 4.3. Experiment #03 and Experiment #11 T08 Heating Curves.
Standoff distance was 4.6" in #03 and 3.6" in #11.

Two experiments having standoff distances of 4.6" (experiment #04) and 3.6" (experiment #12) were compared, as shown in *Figure 4.4*. In both cases,

- Insulation (N)

- Top reflector (Y)

- Side reflectors (Y)

The heating curve was steeper for experiment #12, and the heating time was 20.17 minutes compared with the heating time of 23.15 minutes for experiment #04. This shows that the closer standoff distance resulted in faster heating time.
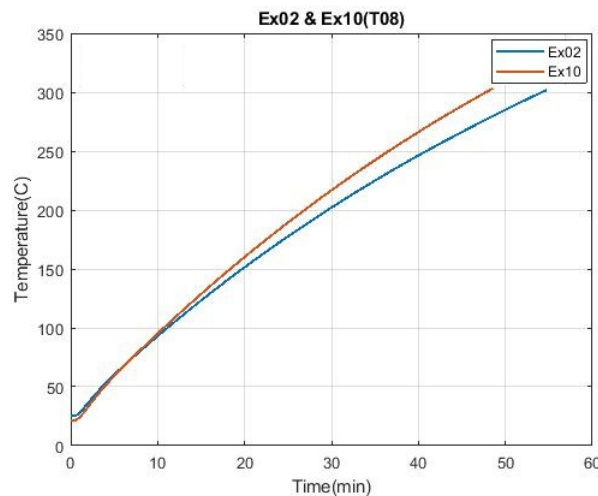
Figure 4.4. Experiment #04 and Experiment #12 T08 Heating Curves.
Standoff distance was 4.6" in #04 and 3.6" in #12.

Two experiments having standoff distances of 4.6" (experiment #05) and 3.6"
(experiment #13) were compared, as shown in *Figure 4.5*. In both cases,

- Insulation (Y)

- Top reflector (Y)

- Side reflectors (Y)

The heating curve was steeper for experiment #12, and the heating time was 19.87
minutes compared with the heating time of 21.45 minutes for experiment #05. This shows
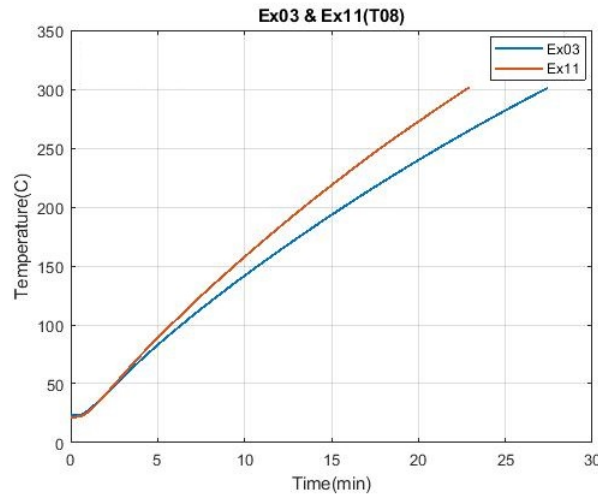that the closer standoff distance resulted in faster heating time.

Figure 4.5. Experiment #05 and Experiment #13 T08 Heating Curves.
Standoff distance was 4.6" in #05 and 3.6" in #13.

Two experiments having standoff distances of 4.6" (experiment #06) and 3.6" (experiment #14) were compared, as shown in *Figure 4.6*. In both cases,

- Insulation (Y)

- Top reflector (N)

- Side reflectors (Y)

The heating curve was steeper for experiment #14, and the heating time was 42.65 minutes compared with the heating time of 47.88 minutes for experiment #06. This shows that the closer standoff distance resulted in faster heating time.
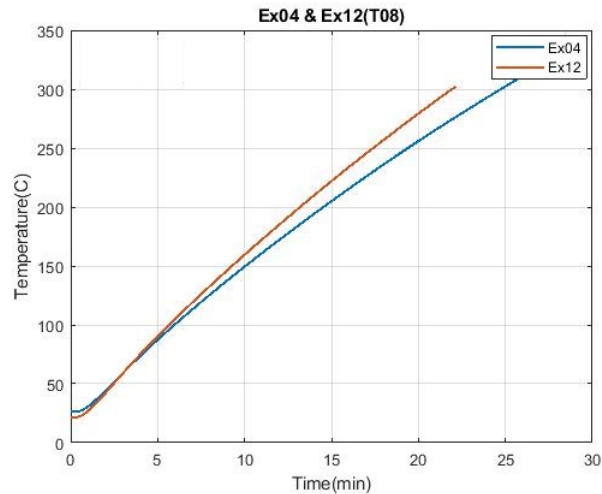
Figure 4.6. Experiment #06 and Experiment #14 T08 Heating Curves.
Standoff distance was 4.6" in #06 and 3.6" in #14.

Two experiments having standoff distances of 4.6" (experiment #07) and 3.6" (experiment #15) were compared, as shown in *Figure 4.7*. In both cases,

- Insulation (Y)

- Top reflector (Y)

- Side reflectors (N)

The heating curve was steeper for experiment #15, and the heating time was 21.35 minutes compared with the heating time of 24.6 minutes for experiment #07. This shows that the closer standoff distance resulted in faster heating time.
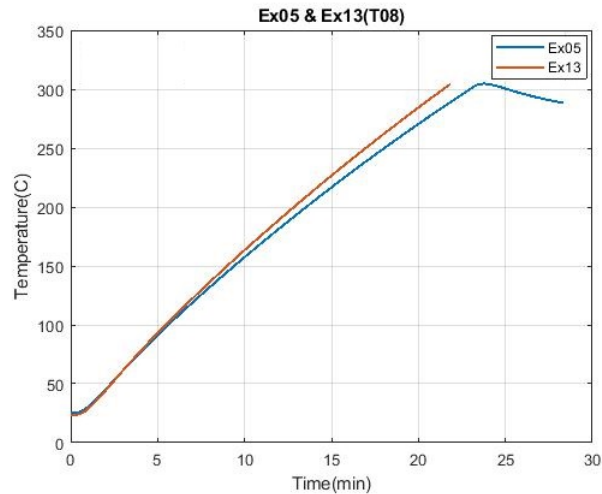
Figure 4.7. Experiment #7 and Experiment #15 T08 Heating Curves. Standoff distance was 4.6" in #7 and 3.6" in #15.

Two experiments having standoff distances of 4.6" (experiment #08) and 3.6" (experiment #16) were compared, as shown in *Figure 4.8.* In both cases,

- Insulation (Y)

- Top reflector (N)

- Side reflectors (N)

The heating curve was steeper for experiment #16, and the heating time was 43.85 minutes compared with the heating time of 49.77 minutes for experiment #08. This shows that the closer standoff distance resulted in faster heating time.
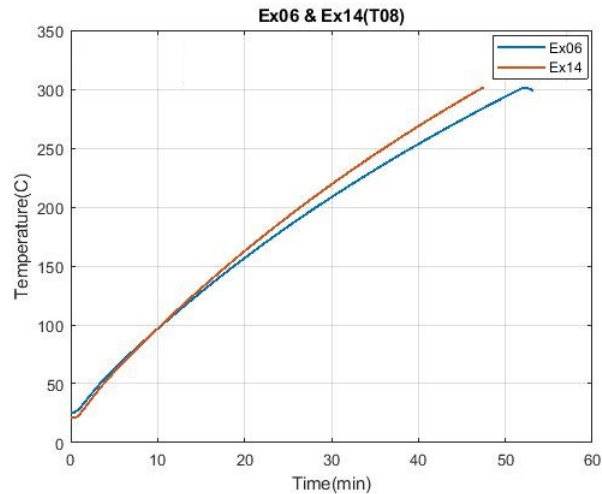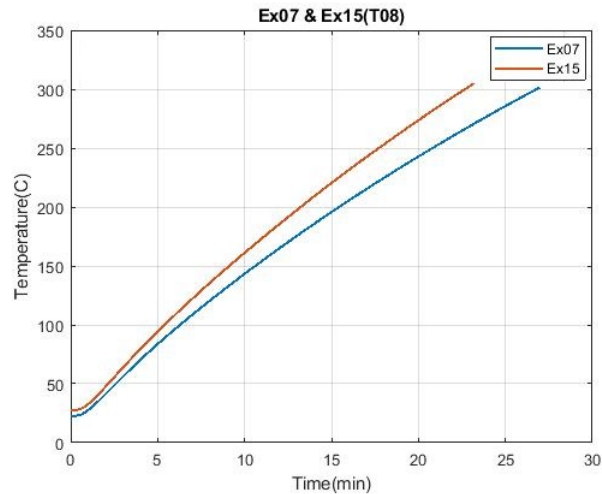
Figure 4.8. Experiment #8 and Experiment #16 T08 Heating Curves. Standoff distance was 4.6" in #8 and 3.6" in #16.

4.2.2 Usage of insulation

Two experiments having no insulation (experiment #01) and insulation (experiment #08) were compared, as shown in *Figure 4.9.* In both cases,

- Distance (4.6")

- Top reflector (N)

- Side reflectors (N)

The heating curve was steeper for experiment #08, and the heating time was 49.77 minutes compared with the heating time of 53.4 minutes for experiment #01. This shows that using insulation resulted in faster heating time.
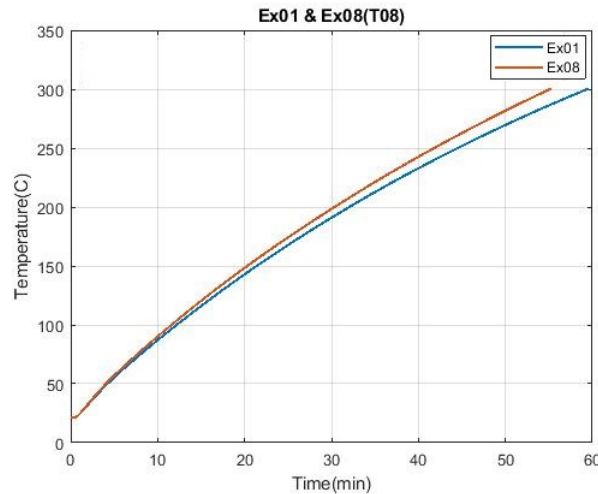
Figure 4.9. Experiment #01 and Experiment #08 T08 Heating Curves.
Insulation was nonexistent in #01 and existent in #08.

Two experiments having no insulation (experiment #02) and insulation
(experiment #06) were compared, as shown in *Figure 4.10*. In both cases,

- Distance (4.6")

- Top reflector (N)

- Side reflectors (Y)

The heating curve was steeper for experiment #06, and the heating time was 47.88
minutes compared with the heating time of 49.88 minutes for experiment #02. This shows
that using insulation resulted in faster heating time.

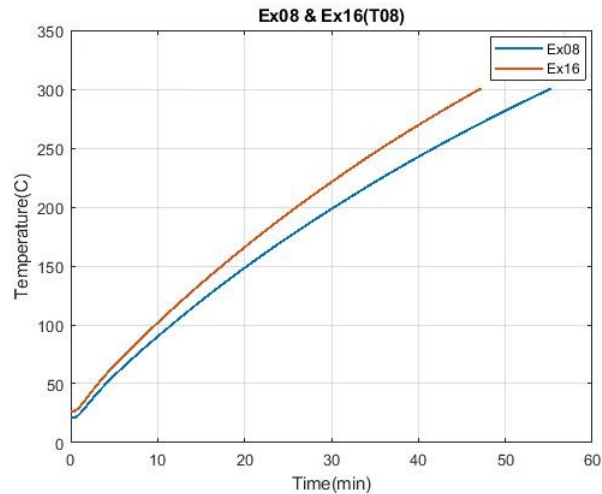*Figure 4.10.* Experiment #02 and Experiment #06 T08 Heating Curves. Insulation was nonexistent in #02 and existent in #06.

Two experiments having no insulation (experiment #03) and insulation (experiment #07) were compared, as shown in *Figure 4.11*. In both cases,

- Distance (4.6")

- Top reflector (Y)

- Side reflectors (N)

The heating curve was steeper for experiment #07, and the heating time was 24.6 minutes compared with the heating time of 25.07 minutes for experiment #03. Although this shows that using insulation resulted in faster heating time, the heating curves and time are extremely similar, and it is unclear if the difference in heating time is significant.

Figure 4.11. Experiment #03 and Experiment #07 T08 Heating Curves.
Insulation was nonexistent in #03 and existent in #07.

Two experiments having no insulation (experiment #04) and insulation
(experiment #05) were compared, as shown in *Figure 4.12*. In both cases,

- Distance (4.6")

- Top reflector (Y)

- Side reflectors (Y)

The heating curve was steeper for experiment #05, and the heating time was 21.45
minutes compared with the heating time of 23.15 minutes for experiment #04. This shows
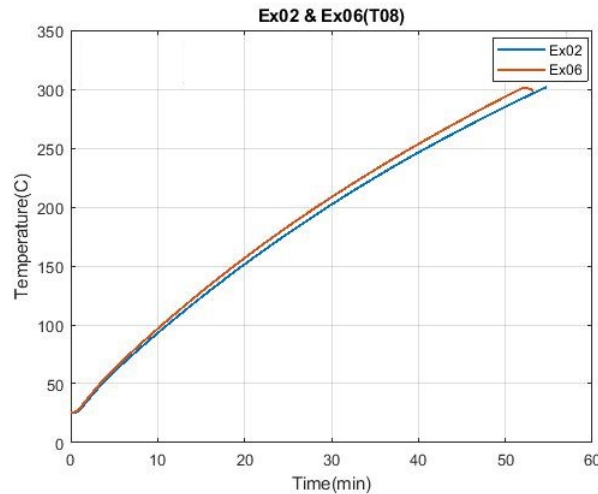that using insulation resulted in faster heating time.

Figure 4.12. Experiment #04 and Experiment #05 T08 Heating Curves.
Insulation was nonexistent in #04 and existent in #05.

Two experiments having no insulation (experiment #09) and insulation
(experiment #16) were compared, as shown in *Figure 4.13*. In both cases,

- Distance (3.6")

- Top reflector (N)

- Side reflectors (N)

The heating curve was steeper for experiment #09, and the heating time was 42.5 minutes
compared with the heating time of 43.85 minutes for experiment #16. This shows that
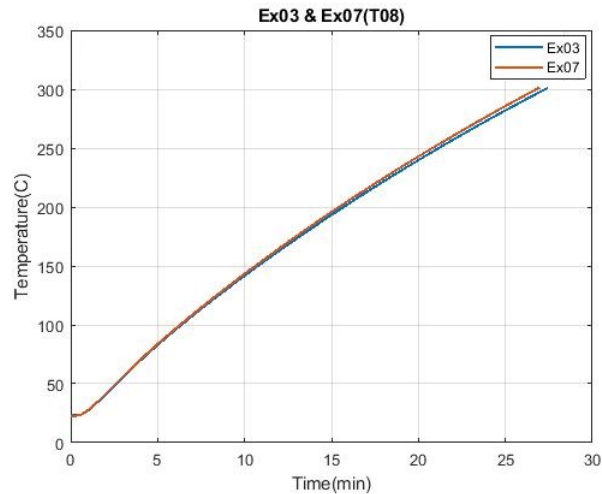using insulation resulted in slower heating time.

Figure 4.13. Experiment #09 and Experiment #16 T08 Heating Curves.
Insulation was nonexistent in #09 and existent in #16.

Two experiments having no insulation (experiment #10) and insulation (experiment #14) were compared, as shown in *Figure 4.14*. In both cases,

- Distance (3.6")

- Top reflector (N)

- Side reflectors (Y)

The heating curve was steeper for experiment #14, and the heating time was 42.65 minutes compared with the heating time of 43.25 minutes for experiment #10. Although this shows that using insulation resulted in faster heating time, the heating curves and time are extremely similar, and it is unclear if the difference in heating time is significant.
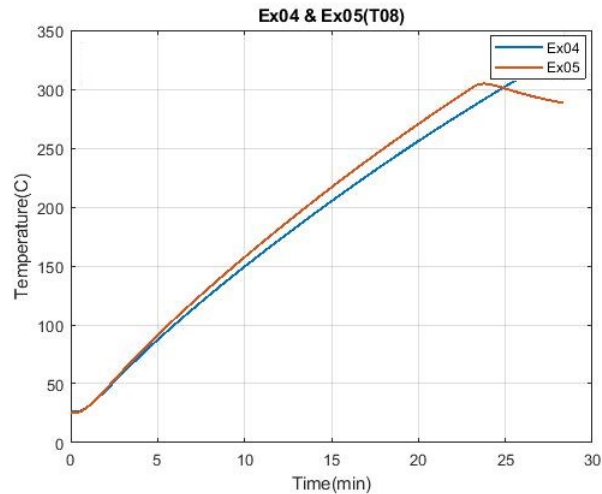
Figure 4.14. Experiment #10 and Experiment #14 T08 Heating Curves.
Insulation was nonexistent in #10 and existent in #14.

Two experiments having no insulation (experiment #11) and insulation
(experiment #15) were compared, as shown in *Figure 4.15*. In both cases,

- Distance (3.6")

- Top reflector (Y)

- Side reflectors (N)

The heating curve was steeper for experiment #11, and the heating time was 20.8 minutes
compared with the heating time of 21.35 minutes for experiment #15. In this case using
insulation resulted in a slower heating time, however the heating curves and time are
extremely similar, and it is unclear if the difference in heating time is significant.
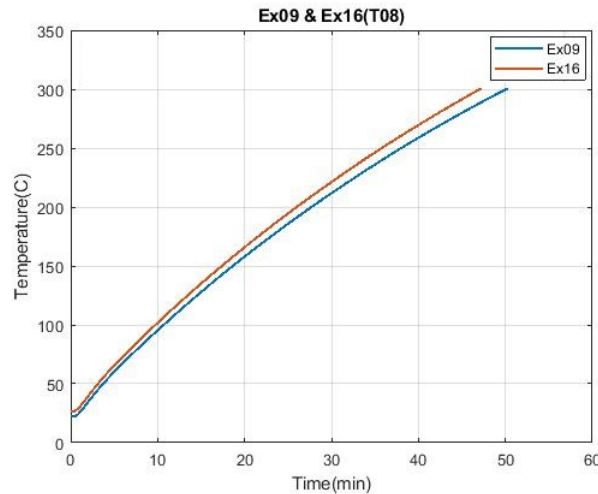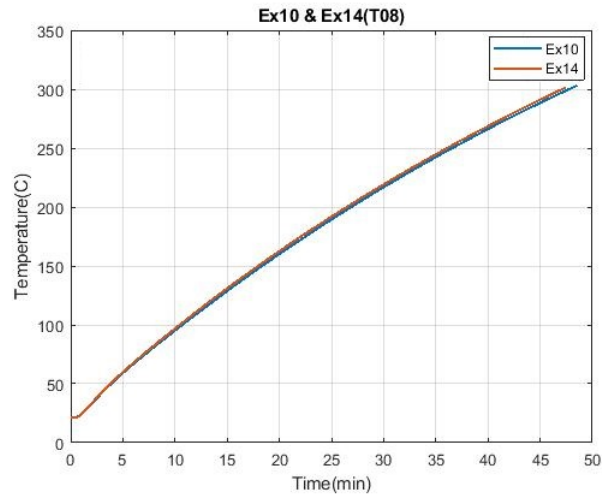
Figure 4.15. Experiment #11 and Experiment #15 T08 Heating Curves. Insulation was nonexistent in #11 and existent in #15.

Two experiments having no insulation (experiment #12) and insulation (experiment #13) were compared, as shown in *Figure 4.16*. In both cases,

- Distance (3.6")

- Top reflector (Y)

- Side reflectors (Y)

The heating curve was steeper for experiment #13, and the heating time was 19.87 minutes compared with the heating time of 20.17 minutes for experiment #12. Although this shows that using insulation resulted in faster heating time, the heating curves and time are extremely similar, and it is unclear if the difference in heating time is significant.
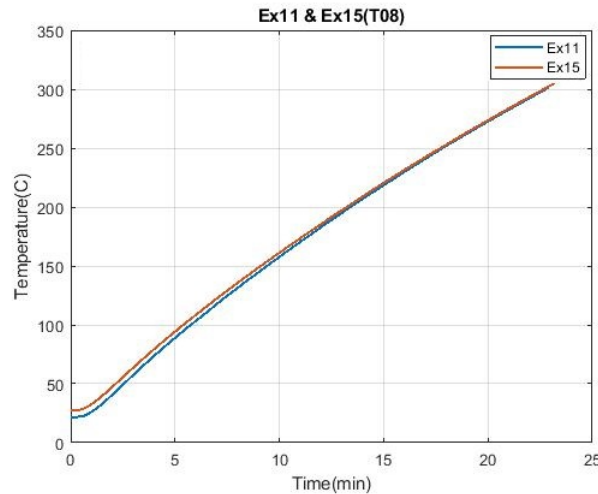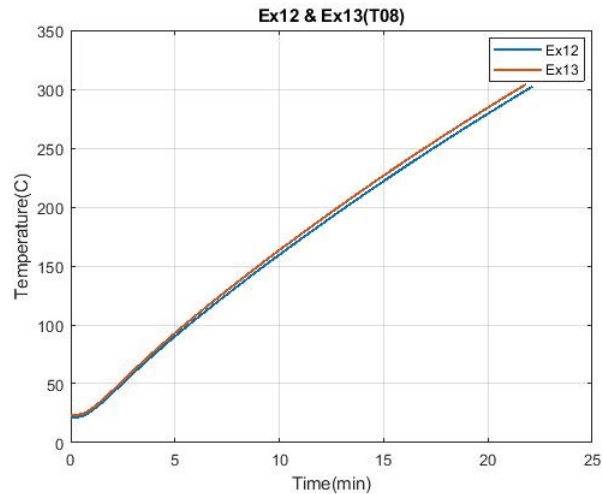
Figure 4.16. Experiment #12 and Experiment #13 T08 Heating Curves.
Insulation was nonexistent in #12 and existent in #13.

4.2.3 Utilization of top reflector

Two experiments having no top reflector (experiment #01) and top reflector
(experiment #03) were compared, as shown in *Figure 4.17*. In both cases,

- Distance (4.6")

- Insulation (N)

- Side reflectors (N)

The heating curve was steeper for experiment #03, and the heating time was 25.07
minutes compared with the heating time of 53.4 minutes for experiment #01. This shows
that using top reflector resulted in faster heating time.
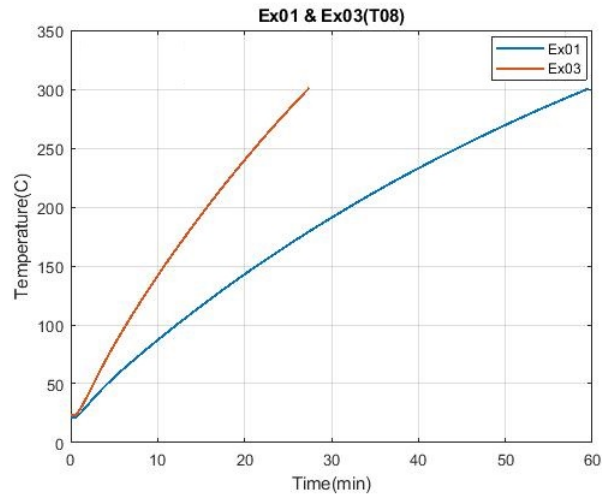
Figure 4.17. Experiment #01 and Experiment #03 T08 Heating Curves. Top reflector was not used in #01 and used in #03.

Two experiments having no top reflector (experiment #02) and top reflector (experiment #04) were compared, as shown in *Figure 4.18*. In both cases,

- Distance (4.6")

- Insulation (N)

- Side reflectors (Y)

The heating curve was steeper for experiment #04, and the heating time was 23.15 minutes compared with the heating time of 49.88 minutes for experiment #02. This shows that using top reflector resulted in faster heating time.

Figure 4.18. Experiment #02 and Experiment #04 T08 Heating Curves. Top reflector was not used in #02 and used in #04.

Two experiments having no top reflector (experiment #06) and top reflector (experiment #05) were compared, as shown in *Figure 4.19*. In both cases,

- Distance (4.6")

- Insulation (Y)

- Side reflectors (Y)

The heating curve was steeper for experiment #05, and the heating time was 21.45 minutes compared with the heating time of 47.88 minutes for experiment #06. This shows that using top reflector resulted in faster heating time.

Figure 4.19. Experiment #06 and Experiment #05 T08 Heating Curves. Top reflector was not used in #06 and used in #05.

Two experiments having no top reflector (experiment #08) and top reflector (experiment #07) were compared, as shown in *Figure 4.20.* In both cases,

- Distance (4.6")

- Insulation (Y)

- Side reflectors (N)

The heating curve was steeper for experiment #07, and the heating time was 24.6 minutes compared with the heating time of 49.77 minutes for experiment #08. This shows that using top reflector resulted in faster heating time.
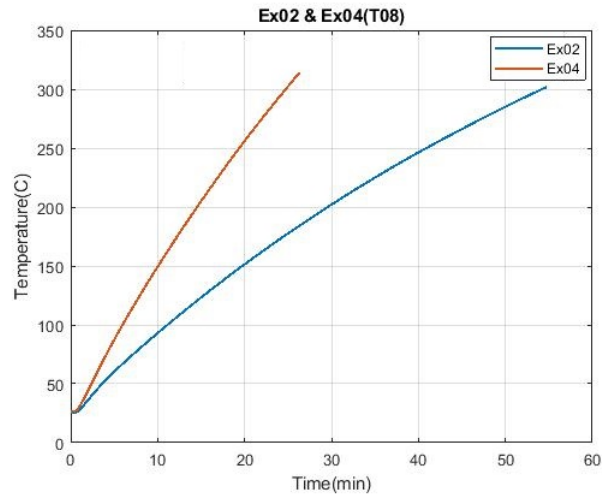
Figure 4.20. Experiment #08 and Experiment #07 T08 Heating Curves. Top reflector was not used in #08 and used in #07.

Two experiments having no top reflector (experiment #09) and top reflector (experiment #11) were compared, as shown in *Figure 4.21*. In both cases,

- Distance (3.6")

- Insulation (N)

- Side reflectors (N)

The heating curve was steeper for experiment #11, and the heating time was 20.8 minutes compared with the heating time of 42.5 minutes for experiment #09. This shows that using top reflector resulted in faster heating time.

Figure 4.21. Experiment #09 and Experiment #11 T08 Heating Curves. Top reflector was not used in #09 and used in #11.

Two experiments having no top reflector (experiment #10) and top reflector (experiment #12) were compared, as shown in *Figure 4.22*. In both cases,

- Distance (3.6")

- Insulation (N)

- Side reflectors (Y)

The heating curve was steeper for experiment #12, and the heating time was 20.17 minutes compared with the heating time of 43.25 minutes for experiment #10. This shows that using top reflector resulted in faster heating time.
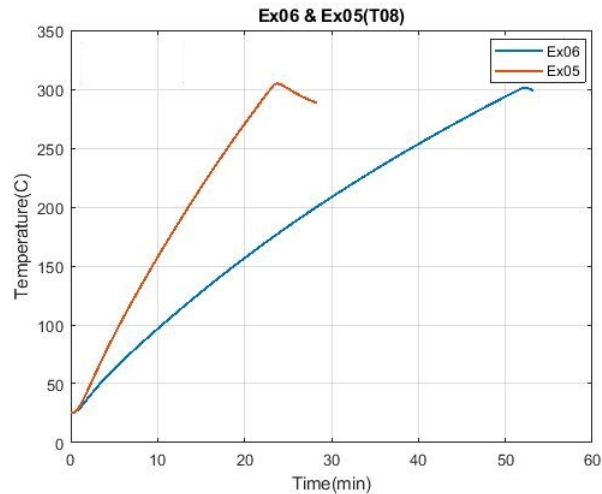
Figure 4.22. Experiment #10 and Experiment #12 T08 Heating Curves. Top reflector was not used in #10 and used in #12.

Two experiments having no top reflector (experiment #14) and top reflector (experiment #13) were compared, as shown in *Figure 4.23*. In both cases,

- Distance (3.6")

- Insulation (Y)

- Side reflectors (Y)

The heating curve was steeper for experiment #13, and the heating time was 19.87 minutes compared with the heating time of 42.65 minutes for experiment #14. This shows that using top reflector resulted in faster heating time.
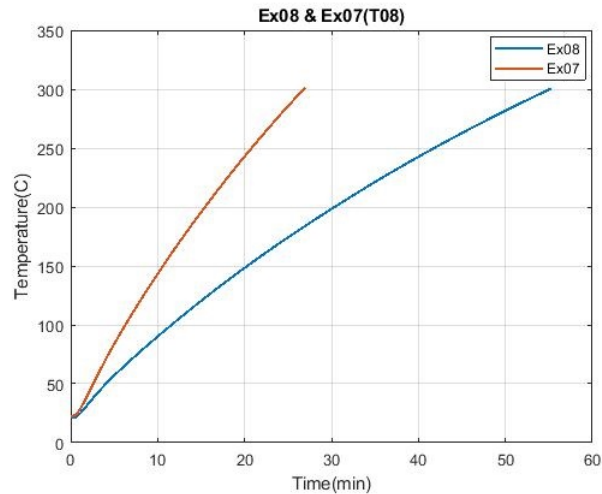
Figure 4.23. Experiment #14 and Experiment #13 T08 Heating Curves. Top reflector was not used in #14 and used in #13.

Two experiments having no top reflector (experiment #16) and top reflector (experiment #15) were compared, as shown in *Figure 4.24*. In both cases,

- Distance (3.6")

- Insulation (Y)

- Side reflectors (N)

The heating curve was steeper for experiment #15, and the heating time was 21.35 minutes compared with the heating time of 43.85 minutes for experiment #16. This shows that using top reflector resulted in faster heating time.

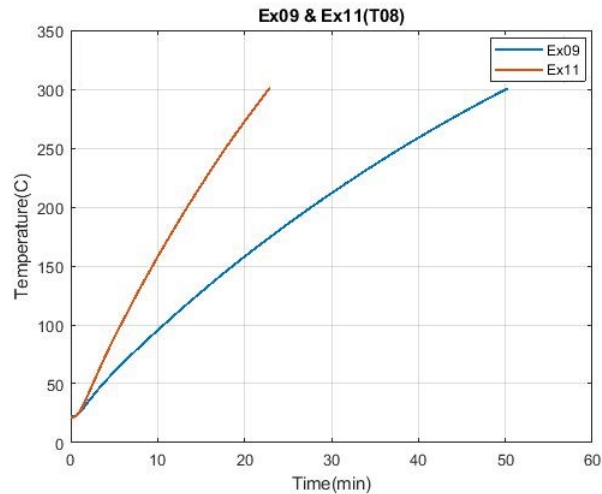*Figure 4.24.* Experiment #16 and Experiment #05 T08 Heating Curves. Top reflector was not used in #16 and used in #15.

4.2.4 Utilization of side reflectors

Two experiments having no side reflector (experiment #01) and side reflector (experiment #02) were compared, as shown in *Figure 4.25*. In both cases,

- Distance (4.6")

- Insulation (N)

- Top reflector (N)

The heating curve was steeper for experiment #02, and the heating time was 49.88 minutes compared with the heating time of 53.4 minutes for experiment #01. This shows that using side reflectors resulted in faster heating time.
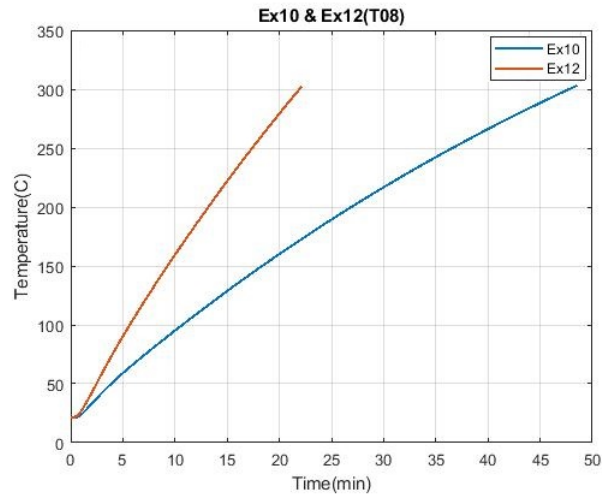
Figure 4.25. Experiment #01 and Experiment #02 T08 Heating Curves. Side reflector was not used in #01 and used in #02.

Two experiments having no side reflector (experiment #03) and side reflector (experiment #04) were compared, as shown in *Figure 4.26*. In both cases,

- Distance (4.6")

- Insulation (N)

- Top reflector (Y)

The heating curve was steeper for experiment #04, and the heating time was 23.15 minutes compared with the heating time of 25.07 minutes for experiment #03. This shows that using side reflectors resulted in faster heating time.
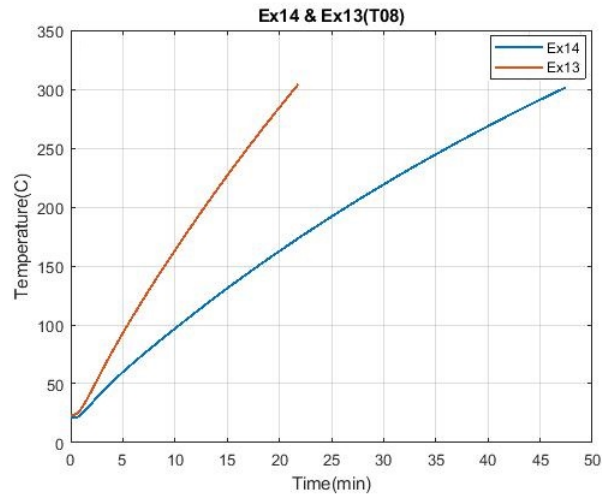
Figure 4.26. Experiment #03 and Experiment #04 T08 Heating Curves. Side reflector was not used in #03 and used in #04.

Two experiments having no side reflector (experiment #07) and side reflector (experiment #05) were compared, as shown in *Figure 4.27*. In both cases,

- Distance (4.6")

- Insulation (Y)

- Top reflector (Y)

The heating curve was steeper for experiment #05, and the heating time was 21.45 minutes compared with the heating time of 24.6 minutes for experiment #07. This shows that using side reflectors resulted in faster heating time.

Figure 4.27. Experiment #07 and Experiment #05 T08 Heating Curves. Side reflector was not used in #07 and used in #05.

Two experiments having no side reflector (experiment #08) and side reflector (experiment #06) were compared, as shown in *Figure 4.28.* In both cases,

- Distance (4.6")

- Insulation (Y)

- Top reflector (N)

The heating curve was steeper for experiment #06, and the heating time was 47.88 minutes compared with the heating time of 49.77 minutes for experiment #08. This shows that using side reflectors resulted in faster heating time.
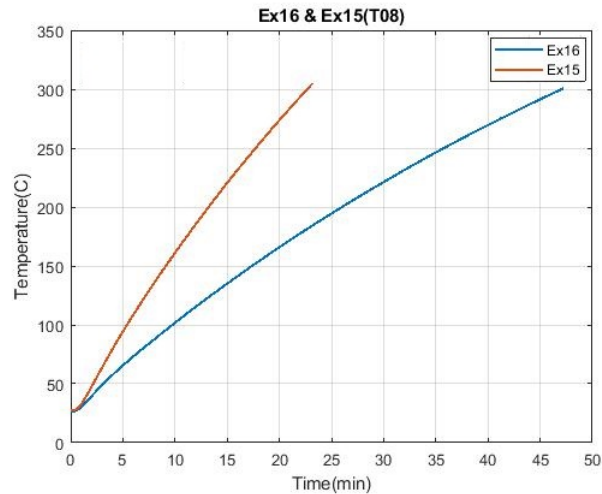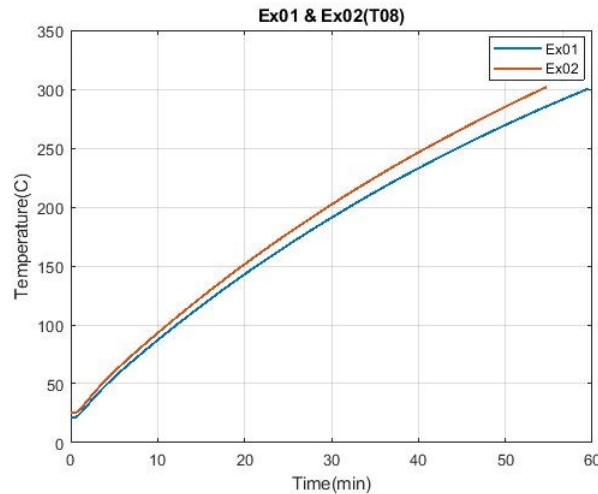
Figure 4.28. Experiment #08 and Experiment #06 T08 Heating Curves. Side reflector was not used in #08 and used in #06.

Two experiments having no side reflector (experiment #09) and side reflector (experiment #10) were compared, as shown in *Figure 4.29.* In both cases,

- Distance (3.6")

- Insulation (N)

- Top reflector (N)

The heating curve was steeper for experiment #09, and the heating time was 42.5 minutes compared with the heating time of 43.25 minutes for experiment #10. This shows that using side reflectors resulted in slower heating time, but the heating curves and time are very similar, it is unclear if the difference in heating time is significant.
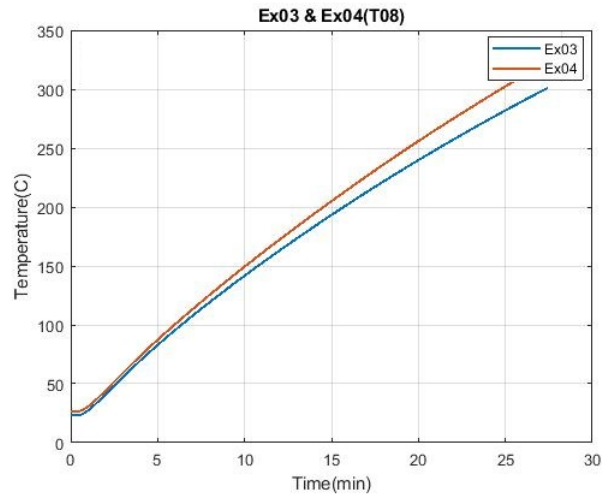
Figure 4.29. Experiment #09 and Experiment #10 T08 Heating Curves. Side reflector was not used in #09 and used in #10.

Two experiments having no side reflector (experiment #11) and side reflector (experiment #12) were compared, as shown in *Figure 4.30.* In both cases,

- Distance (3.6")

- Insulation (N)

- Top reflector (Y)

The heating curve was steeper for experiment #12, and the heating time was 20.17 minutes compared with the heating time of 20.8 minutes for experiment #11. This shows that using side reflectors resulted in faster heating time, but the heating curves and time are very similar, it is unclear if the difference in heating time is significant.
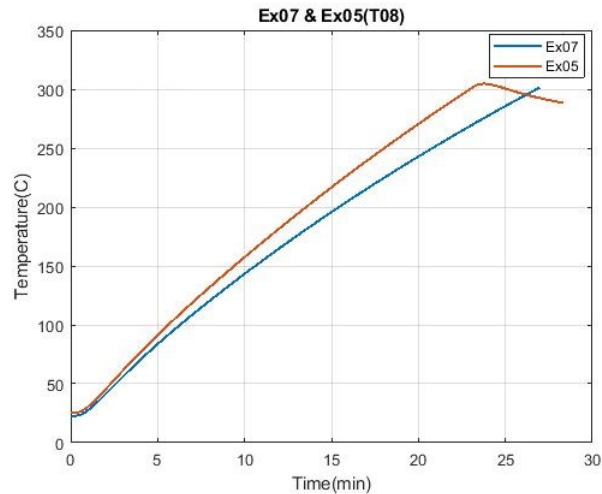
Figure 4.30. Experiment #11 and Experiment #12 T08 Heating Curves. Side reflector was not used in #11 and used in #12.

Two experiments having no side reflector (experiment #15) and side reflector (experiment #13) were compared, as shown in *Figure 4.31*. In both cases,

- Distance (3.6")

- Insulation (Y)

- Top reflector (Y)

The heating curve was steeper for experiment #13, and the heating time was 19.87 minutes compared with the heating time of 21.35 minutes for experiment #15. This shows that using side reflectors resulted in faster heating time.
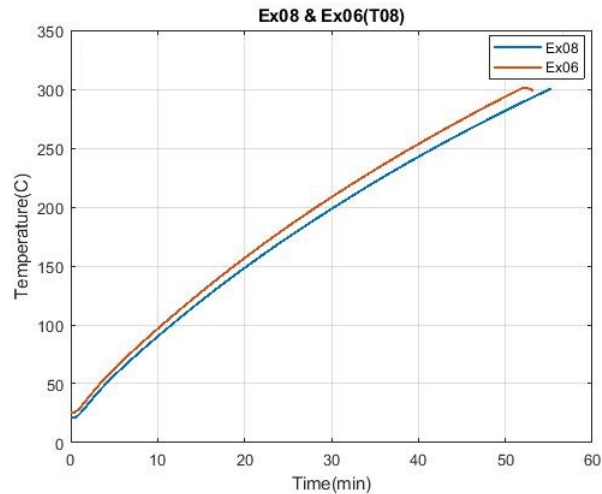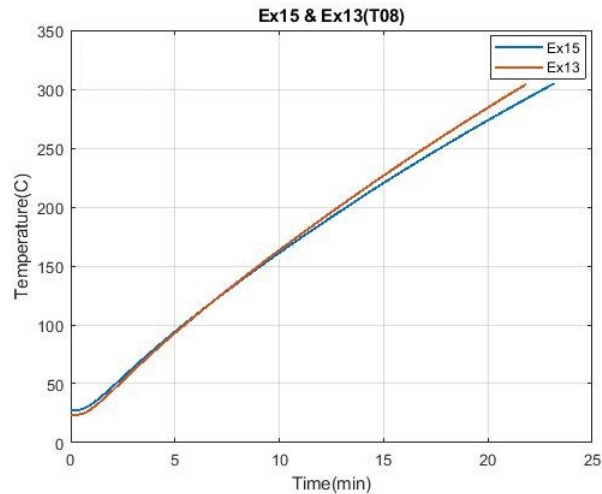
Figure 4.31. Experiment #15 and Experiment #13 T08 Heating Curves. Side reflector was not used in #15 and used in #13.

Two experiments having no side reflector (experiment #16) and side reflector (experiment #14) were compared, as shown in *Figure 4.32*. In both cases,

- Distance (3.6")

- Insulation (Y)

- Top reflector (N)

The heating curve was steeper for experiment #14, and the heating time was 42.65 minutes compared with the heating time of 43.85 minutes for experiment #16. This show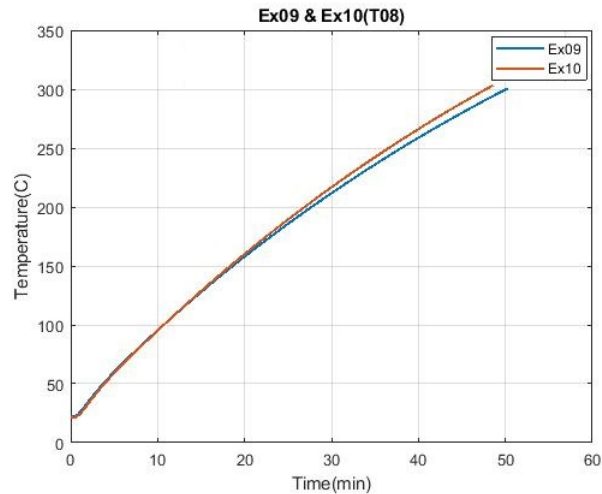s that using side reflectors resulted in faster heating time, but the heating curves and time are very similar, and it is unclear if the difference in heating time is significant.
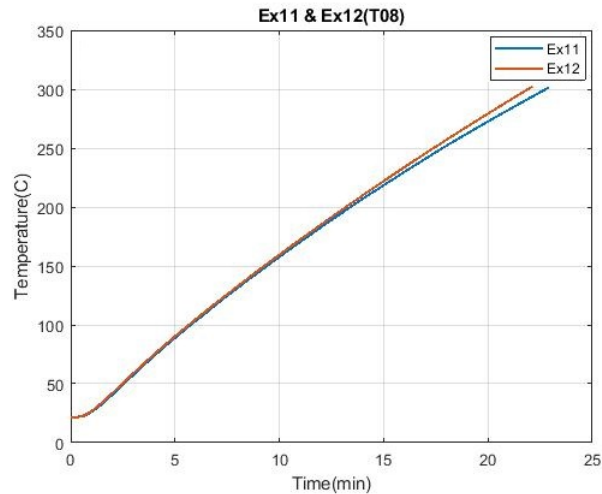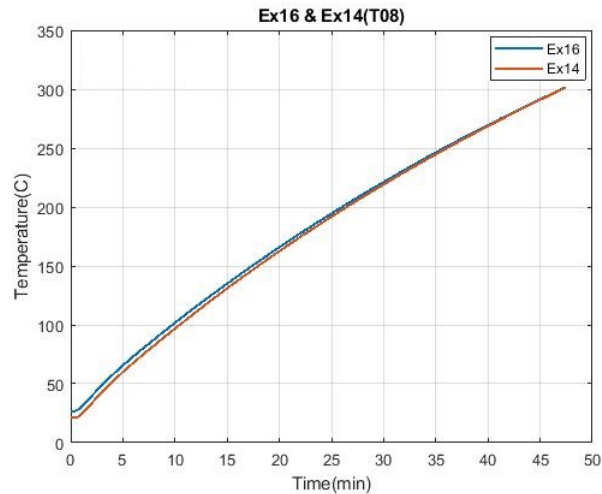
Figure 4.32. Experiment #16 and Experiment #14 T08 Heating Curves. Side reflector was not used in #16 and used in #14.

4.3 Discussion of Variables

4.3.1 Distance

Reviewing the compiled data, the heater distance clearly has an effect on the heating performance. This is expected, and agrees with the calculated results. As the standoff distance decreases, the view factor increases which will result in more heat being transferred to the heated surface. Looking at the comparisons, an increase in heating performance can be observed across the results at the closer distance of 3.6" relative to the further 4.6".

4.3.2 Insulation

Attempts in reducing heat losses through convection of the exposed surfaces around and under the die did had some effect as results show, mostly bringing minimal reductions to heating time. In general, it displayed a slight effectiveness at the further distance of 4.6" relative to the 3.6" vertical distance between the heating element and die surface.

4.3.3 Top Reflector

The flat mirror reflector proves to be the most effective method of increasing performance. It effectively converts the bi-directional heater to a uni-directional setup, and was theoretically estimated to double the die surface heat flux, which was closely matched in actual experimentation indicated by the effectively halved heating time in reaching a temperature delta of 260 °C across all comparisons.

4.3.4 Side Reflectors

Side reflectors showed no significant effect on the heating time at the closer distance of 3.6", but do show some effect at the further 4.6" distance. This shows that the side reflectors do indeed have a slight effect in reducing heating losses at further distances, while at the closer distance losses are not as significant and their effect is almost negligible given the already minimal effect in heating performance at the further distance.

4.4 Grouped comparisons

To provide a better visual representation of the results, this section will provide a set of four comparison bar graphs grouping the usage of each variable and comparing the heating times without and with the utilization of said variable. The average heating times of each group is also displayed for better reference.

4.4.1 Distance

Figure 4.33 categorizes results into two groups comparing the effects of heating distance, on the left are heating times obtained at a distance of 4.6 inches, while the right displays the times at a distance of 3.6 inches. The bars are paired corresponding to the experiment setups, so it solely compares the effects of standoff distance as all other available variables are kept consistent. The average heating time was 36.9 minutes for a standoff distance of 4.6" and was 31.8 minutes for a standoff distance of 3.6".
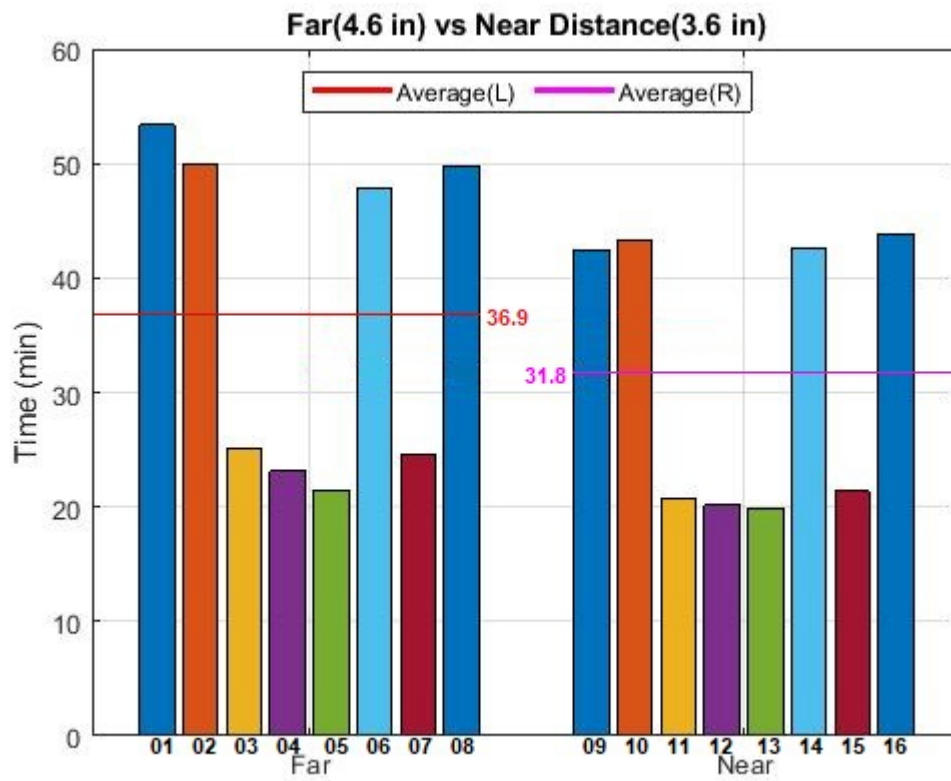
Figure 4.33. Effects of heating distance

<center>4.4.2 Insulation</center>

Figure 4.34 categorizes the results into two groups comparing the effects of insulation on heating time. The bars are paired corresponding to the experiment setups, so it is solely comparing the effects of using insulation and not using insulation. The average heating time was 34.8 minutes for not using insulation and was 33.9 minutes for using insulation.
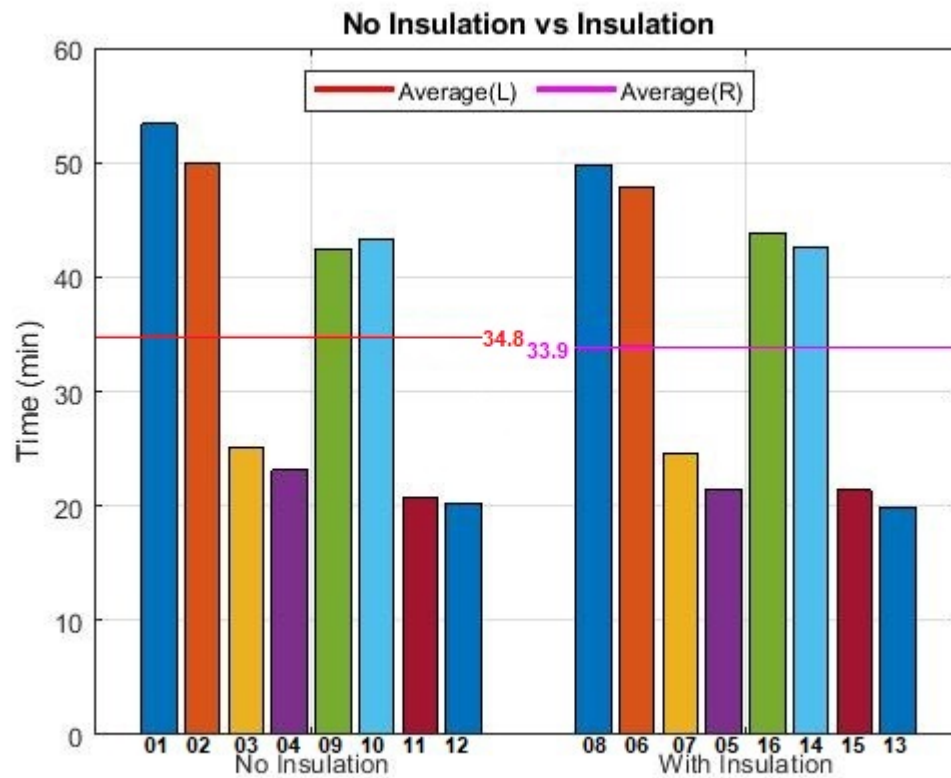
<center>*Figure 4.34.* Effects of insulation</center>

4.4.3 Top reflector

Figure 4.35 categorizes the results into two groups comparing the effects of a flat top reflector, The bars are paired corresponding to the experiment setups, so it is solely comparing the effects of using and not using a flat top reflector. Average heating times are shown across each category in minutes. The average heating time was 46.6 minutes for not using the top reflector and was 22.1 minutes for using the top reflector.
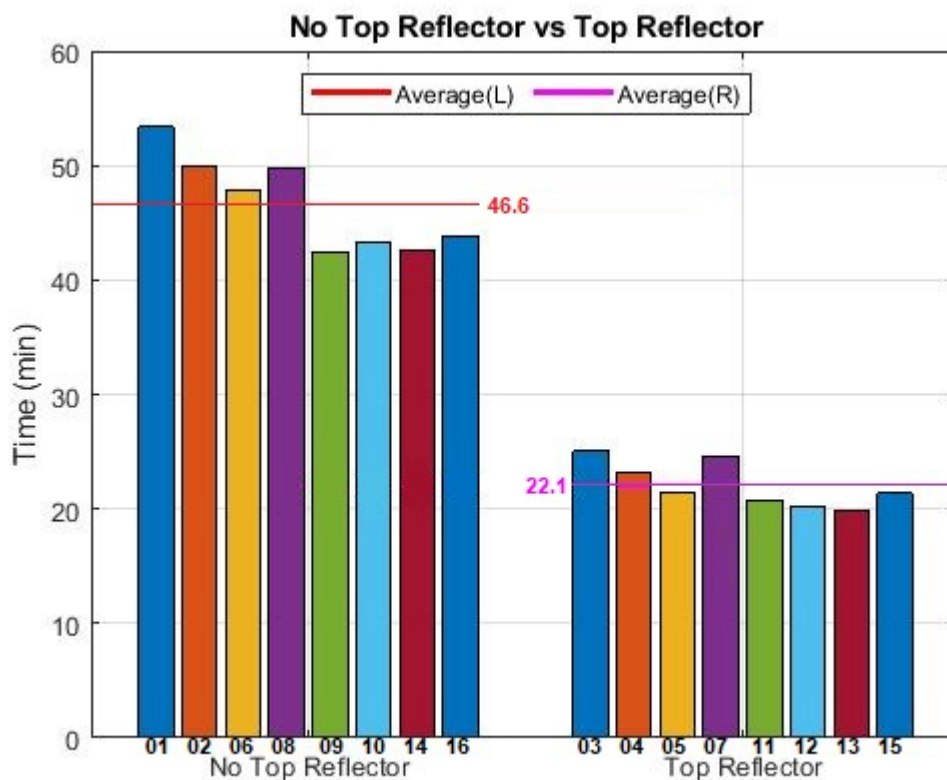
Figure 4.35. Effects of top reflector

4.4.4 Side reflectors

Figure 4.36 categorizes the results into two groups comparing the effects of a pair of side reflectors. The bars are paired corresponding to the experiment setups, so it is solely comparing the effects of having and not having side reflectors. Average heating times are shown across each category in minutes. The average heating time was 35.2 minutes for not using side reflectors and was 33.5 minutes for using side reflectors.
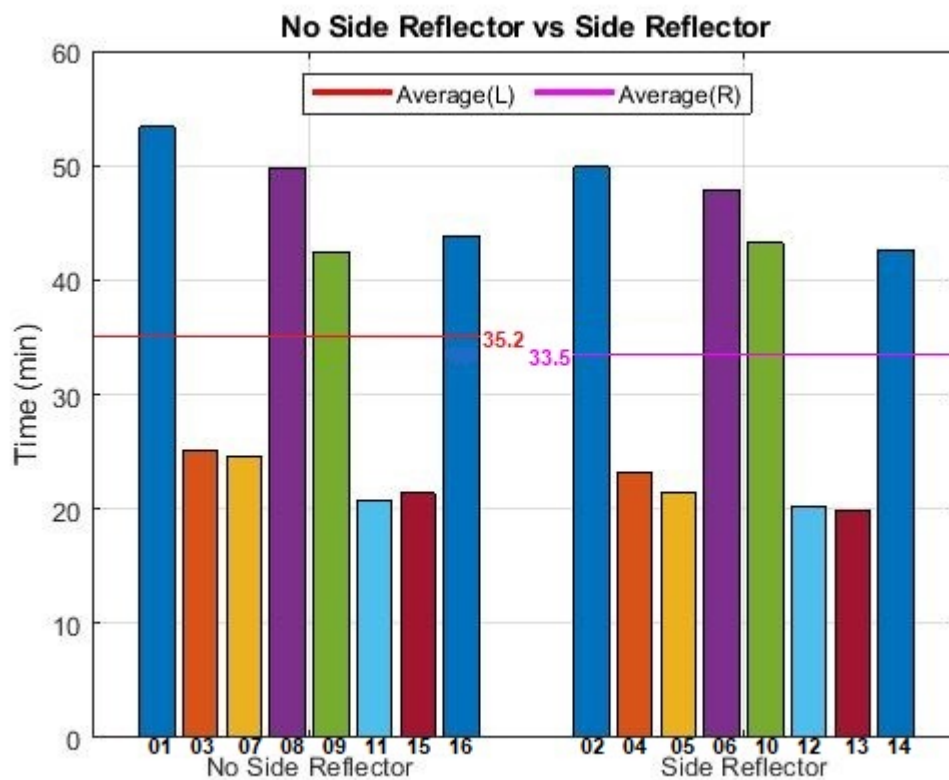
Figure 4.36. Effects of side reflector

<u>4.5 Independent two-sample T-test</u>

To better showcase the respective effectiveness of each evaluated variable, and provide more insight on the significance of the effects on heating performance, an independent two-sample T-test is chosen for statistical analysis. The test was conducted using the data sets comparing the heating times with and without the implementation of each variable, providing two groups with equal sample sizes. The following sub section show tables grouping the results, which correspond to the prior section's graphical representation, followed by the t-test results for each variable.

4.5.1 Distance

Table 4.2 shows experiment results grouped for comparing the effectiveness of heating distance. Table 4.3 shows the T-test results for this comparison.

Table 4.2. Varying standoff distance heating times

Exp # (4.6")	time(min)	Exp # (3.6")	time(min)
1	53.40	9	42.50
2	49.88	10	43.25
3	25.07	11	20.80
4	23.15	12	20.17
5	21.45	13	19.87
6	47.88	14	42.65
7	24.60	15	21.35
8	49.77	16	43.85

Table 4.3. Standoff distance significance, two-Sample t-test assuming equal variances, 95% two-tail

	4.6" distance	3.6" distance
Mean($\bar{x}$)	36.90	31.80
Variance(s^2)	206.58	145.21
Sample size(n)	8	8
Pooled Variance(s_p)	175.90	
df($2n-2$)	14	
t-stat	0.768	
t critical(two-tail)	2.145	

4.5.2 Insulation

Table 4.4 shows experiment results grouped for comparing the effectiveness of using insulation. Table 4.5 shows the T-test results for this comparison.

Table 4.4. Varying insulation heating times

Exp # (NoIns)	time(min)	Exp # (Ins)	time(min)
1	53.40	8	49.77
2	49.88	6	47.88
3	25.07	7	24.60
4	23.15	5	21.45
9	42.50	16	43.85
10	43.25	14	42.65
11	20.80	15	21.35
12	20.17	13	19.87

Table 4.5. Insulation significance, two-Sample t-test assuming equal variances, 95% two-tail

	No insulation	Insulation
Mean($\bar{x}$)	34.78	33.93
Variance(s^2)	192.11	174.11
Sample size(n)	8	8
Pooled Variance(s_p)	183.11	
df($2n-2$)	14	
t-stat	0.126	
t critical(two-tail)	2.145	

4.5.3 Top reflector

Table 4.6 shows experiment results grouped for comparing the effectiveness of using the top reflector. Table 4.7 shows the T-test results for this comparison.

Table 4.6. Varying top reflector heating times

Exp # (NoTR)	time(min)	Exp # (TR)	time(min)
1	53.40	3	25.07
2	49.88	4	23.15
6	47.88	5	21.45
8	49.77	7	24.60
9	42.50	11	20.80
10	43.25	12	20.17
14	42.65	13	19.87
16	43.85	15	21.35

Table 4.7. Top reflector significance, two-Sample t-test assuming equal variances, 95% two-tail

	No top reflector	top reflector
Mean($\bar{x}$)	46.65	22.06
Variance(s^2)	17.12	3.93
Sample size(n)	8	8
Pooled Variance(s_p)	10.53	
df($2n-2$)	14	
t-stat	15.157	
t critical(two-tail)	2.145	

4.5.4 Side reflector

Table 4.8 shows experiment results grouped for comparing the effectiveness of using the top reflector. Table 4.9 shows the T-test results for this comparison.

Table 4.8. Varying side reflector heating times

Exp # (NoSR)	time(min)	Exp # (SR)	time(min)
1	53.40	2	49.88
3	25.07	4	23.15
7	24.60	5	21.45
8	49.77	6	47.88
9	42.50	10	43.25
11	20.80	12	20.17
15	21.35	13	19.87
16	43.85	14	42.65

Table 4.9. Side reflector significance, two-Sample t-test assuming equal variances, 95% two-tail

	No side reflector	side reflector
Mean($\bar{x}$)	35.17	33.54
Variance(s^2)	183.68	181.43
Sample size(n)	8	8
Pooled Variance(s_p)	182.56	
df($2n - 2$)	14	
t-stat	0.241	
t critical(two-tail)	2.145	

4.5.5 Discussion of t-test results

The results of the independent two-sample t-test can provide insight into which variables improved heating performance in a statistically significant manner. The effectiveness of each heating configuration and the resulting t-value form a positive correlation, where a larger t-value directly indicates the higher effectiveness a particular variable has in affecting heating time. Selecting a confidence level of 95%, the critical t-value is 2.145, making the only evaluated variable that presents statistical significance being the top reflector with a t-stat of 15.157, as seen in Table 4.6 and 4.7. Meanwhile the other three variables show a much less significant effect given their t-values all being under 2.145, as can be seen in tables 4.2 and 4.3 for distance, tables 4.4 and 4.5 for insulation, and tables 4.8 and 4.9 for side reflectors. The t-stat for standoff distance was 0.768, the t-stat for insulation was 0.126, and the t-stat for the side reflector was 0.241. While these t-stat values indicate that the variables are not statistically significant, it is useful to observe that the standoff distance had more influence over heating time relative to adding insulation and adding a side reflector. It should also be noted that the results may be affected by the large variance introduced by adding the top reflector, which could well be the lead to lower t-stat values for the other test variables excluding the top reflector.

4.5.6 Additional t-test results excluding top reflector

Considering the large variance values when evaluating variables, an additional t-test was performed excluding the top reflector variable. The following tables 4.10 - 4.12 show the t-test results after removing the data that utilize the top reflector. It can be observed the variance value is greatly reduced and the t-statistic become more representative of the actual effectiveness of the variables. In this case, the standoff distance becomes statistically significant.

Table 4.10. Standoff distance significance excluding top reflector data, two-Sample t-test assuming equal variances, 95% two-tail

	4.6" distance	3.6" distance
Mean($\bar{x}$)	50.23	43.06
Variance(s^2)	5.30	0.38
Sample size(n)	4	4
Pooled Variance(s_p)	2.84	
df($2n-2$)	6	
t-stat	6.019	
t critical(two-tail)	2.447	

Table 4.11. Insulation significance excluding top reflector data, two-Sample
t-test assuming equal variances, 95% two-tail

	No insulation	Insulation
Mean($\bar{x}$)	47.26	46.04
Variance(s^2)	27.77	11.19
Sample size(n)	4	4
Pooled Variance(s_p)	19.48	
df($2n-2$)	6	
t-stat	0.391	
t critical(two-tail)	2.447	

Table 4.12. Side reflector significance excluding top reflector data,
two-Sample t-test assuming equal variances, 95% two-tail

	No side reflector	side reflector
Mean($\bar{x}$)	47.38	45.92
Variance(s^2)	26.07	12.46
Sample size(n)	4	4
Pooled Variance(s_p)	19.27	
df($2n-2$)	6	
t-stat	0.471	
t critical(two-tail)	2.447	

4.6 Answer to Research Question

The initial target window of reaching 300 °C was achievable within the targeted 30 minute range, with varying degrees of performance under the different setups of the heating system. The fastest heating time of 19.87 minutes to reach a temperature delta of +260 °C was achieved in experiment #13, where the standoff distance was at the closer 3.6", insulation, top and side reflectors were also utilized.

4.7 Conclusion

Compiling the data into bar graphs reflects the effects of the four selected variables, providing a visual representation of the effects of each on the heating performance. The usage of the top reflector shows to be the most effective in reducing the overall heating time. The next most effective variable was reducing the standoff distance. Both the effects of insulating the sides of the die and utilizing side reflectors show to be dependent on the heating distance, being more significant at the further distance and less significant at the closer distance.

CHAPTER 5. SUMMARY, CONCLUSIONS, AND RECOMMENDATIONS

5.1 Summary

Aluminum high pressure die casting is a highly valued manufacturing method for the mass production of high quality aluminum alloy parts. It is heavily used in the automotive industry and is responsible for the production of many crucial items such as engine, transmission and suspension components [4]. The process of aluminum HPDC consists of multiple steps, improvements in any step of the process can bring significant savings in resources for the manufacturer, due to the high volume nature of said production [2].

Improving the preheating procedure during a cold start prior to production, and the maintaining of die temperature during machinery downtime can provide significant improvements to the process. Through the use of a dedicated die heater, the reliance on warm up casting cycles can be reduced, effectively reducing the thermal fatigue through lessening the extreme thermal cycling during warm-up [6].

An electric short wave infrared heater was utilized as the heating device in this research project, employing a 36kW bi-directional unit, heating performance was assessed through the measurement of heating time. Adjustment in standoff distance, usage of insulation material, top and side reflector panels were variables chosen to enhance heating performance, they are evaluated by looking at their effectiveness in reducing heating time.

From comparing the average heating time of the experimental results, it was observed that the each of the variables had varying degrees of impact on heating time required to reach the set temperature of 300°C. Among the variables analyzed, the top reflector proved to be the sole variable that provided a statistically significant result in influencing heating time. For the remaining variables, the following order of significance was standoff distance, side reflectors and lastly insulation which was the least effective. These variables although may not be statistically significant, they all displayed varying degrees of effectiveness, a likely reason for their insignificance may be due to the large variance the top reflector brings into the heating times analyzed, this dilutes the effectiveness of the remaining variables and thus they should not be simply overlooked.

5.1.1 Summary of findings

- Utilizing a top mounted reflector running the heater as a uni-directional unit is extremely effective in reducing the time required.

- The standoff distance between the heating element plane and die surface has a significant effect on the time required.

- Side reflectors show slight improvements in heating performance overall, being slightly more effective at the further standoff distance.

- Insulating the exposed sides of the die has minimal to no effect on the time required.

5.2 Conclusions

Electric short wave infrared die heating is a viable method of heating dies used for aluminum high pressure die casting. The proposed initial goal of heating a die surface to 300 degrees Celsius can be achieved using a bi-directional 36kW heater emitting short wave infrared radiation.

At the tested standoff distances, the closer 3.6 inch distance proved to achieve shorter heating times regardless of the use of reflectors and insulation compared to the further 4.6 inch distance.

Convective and conductive losses are minimal under the conditions of the experiment, with insulation and side reflectors showing slight effects at the further distance of 4.6 inches, but with a negligible effect at the closer distance of 3.6 inches.

Using the top reflector proved to be exceptionally effective in decreasing heating times. Converting the bi-directional setup into a uni-directional heater via the use of a flat mirror reflector can nearly double the heating performance, effectively reducing the heating time required to reach the same die temperature with the same heater.

Overall, this research can be viewed as an initial testing stage in the usage of electric short wave infrared heating devices on dies used in aluminum high pressure die casting. Being an early test bed prior to continued research in implementation of such systems in the real world, the primary goal is to gain a rudimentary understanding on the heating performance of this specific heating method and effectiveness of a few heating variables, as well as aid in the model validation of simulation software for predicting heating performance which can be used as a basis for further related endeavors.

5.3 Answer to research question

An electric SWIR heating device is capable of heating a HPDC die specimen to 300°C within 30 minutes. After the utilization of experiment variables aimed to reduce heating times, heating performance was able to be improved to meet and exceed the initial requirements.

5.4 Recommendations

The electric heating system tested in this study is chosen due to its simplicity and flexibility, it can be quickly applied to varying types of die molds, though its effectiveness may vary and customization may be required due to some specific die geometries. There are certainly still many improvements around the topic yet to be explored, continuing work can be done on discovering its actual effect on die service life after the use of heating devices, and the use of localized heating to focus radiation in certain regions of interest for enhanced performance and efficiency. Additionally, whether the usage of such heating systems is economically relevant in production environments also needs further analysis.

5.4.1 Future Work

- Extended testing for a similar heating system in actual production environments is needed for validation of system reliability and longevity, this could be a continuation of the existing study aiming to discover potential issues that may arise.

- Analysis in cost for implementation in a production facility can be done to estimate the return on investment.

- Heating temperature distribution over the surface features of the die can be further researched, locations with excessive temperature need be avoided to reduce the possible annealing affects that may soften the die material over time.

- Heating experiments should be tested in conjunction with die lubricant sprays which are used in aluminum HPDC, so to understand how the cooling effect will change the heating requirements. This will greatly aid in the ability to obtain a more accurate preheating temperature requirement for the die.

- Further research on fine control of the heating system can be explored with the usage of non contact temperature measuring devices, utilization of feedback loops may allow more complex functions via automated control.

LIST OF REFERENCES

[1] Cathal Wilson and Gerard McGranaghan. Infrared heating comes of age. *Reinforced Plastics*, 58(2):43–47, 2014.

[2] Franco Bonollo, Nicola Gramegna, and Giulio Timelli. High-pressure die-casting: Contradictions and challenges. *The Journal of The Minerals, Metals Materials Society (TMS)*, 67(5):901–908, 2015.

[3] Corey Vian. Meetings and interview with Corey Vian from FCA, Oct 2019.

[4] F Casarotto, AJ Franke, and R Franke. High-pressure die-cast (hpdc) aluminium alloys for automotive applications. In *Advanced materials in automotive engineering*, pages 109–149. Elsevier, 2012.

[5] CA Blue, VK Sikka, EK Ohriner, PG Engleman, GF Mochnal, A Underys, WT Wu, MC Maguire, and R Mayer. Infrared heating of forging billets and dies, 1999.

[6] Alastair Long, David Thornhill, Cecil Armstrong, and David Watson. Predicting die life from die temperature for high pressure dies casting aluminium alloy. *Applied Thermal Engineering*, 44:100–107, 2012.

[7] Zvonimir Dadić, Dražen Živković, Nikša Čatipović, and Ivo Marinić-Kragić. Influence of steel preheat temperature and molten casting alloy alsi9cu3 (fe) impact speed on wear of x38crmov5-1 steel in high pressure die casting conditions. *Wear*, 424:15–22, 2019.

[8] Yoshiharu Namba. Specular spectral reflectance of aisi304 stainless steel at near-normal incidence. In *Scattering in Optical Materials II*, volume 362, pages 93–103. International Society for Optics and Photonics, 1983.

[9] Chang-Da Wen. Investigation of steel emissivity behaviors: Examination of multispectral radiation thermometry (mrt) emissivity models. *International Journal of Heat and Mass Transfer*, 53(9-10):2035–2043, 2010.

[10] ASHRAE Handbook-HVAC ASHRAE. Ashrae handbook: Heating, ventilating, and air-conditioning systems and equipment. *American Society of Heating Refrigerating and Air-Conditioning Engineers*, 2012.

[11] J Walker, D Hebble, and R Holdren. What is the best method for preheating 4130? *Welding journal*, 93(1):52–56, 2014.

[12] EH Schulte. Impingement heat-transfer rates from torch flames. *Journal of Heat Transfer*, 94(2):231–233, 1972.

[13] Yunus Cengel. *Heat and mass transfer: fundamentals and applications*. McGraw-Hill Higher Education, 2014.

[14] Yan Guanghua, Huang Xinmin, Wang Yanqing, Qin Xingguo, Yang Ming, Chu Zuoming, and Jin Kang. Effects of heat treatment on mechanical properties of h13 steel. *Metal Science and Heat Treatment*, 52(7-8):393–395, 2010.

[15] Minwoo Kang, Gyujin Park, Jae-Gil Jung, Byung-Hoon Kim, and Young-Kook Lee. The effects of annealing temperature and cooling rate on carbide precipitation behavior in h13 hot-work tool steel. *Journal of Alloys and Compounds*, 627:359–366, 2015.

[16] GK Malikov, DL Lobanov, KY Malikov, VG Lisienko, R Viskanta, and AG Fedorov. Direct flame impingement heating for rapid thermal materials processing. *International journal of heat and mass transfer*, 44(9):1751–1758, 2001.

[17] Inc. Ushio America. Qih quartz infrared heater, Aug 2018.

[18] Filippo De Monte and James V. Beck. X22b10t0 slab with jump in heat flux at one boundary, zero heat flux at other boundary and initially at zero temperature. 2013.

[19] LLC MatWeb. Material property data. *URL: http://www. matweb. com (Stand 30.08. 2013)*, 2013.

APPENDIX A. EXPERIMENT DATA

Note: T0-T10 show temperature probe measurements from varying locations within the die, while T11 and T12 show enclosure and ambient temperatures
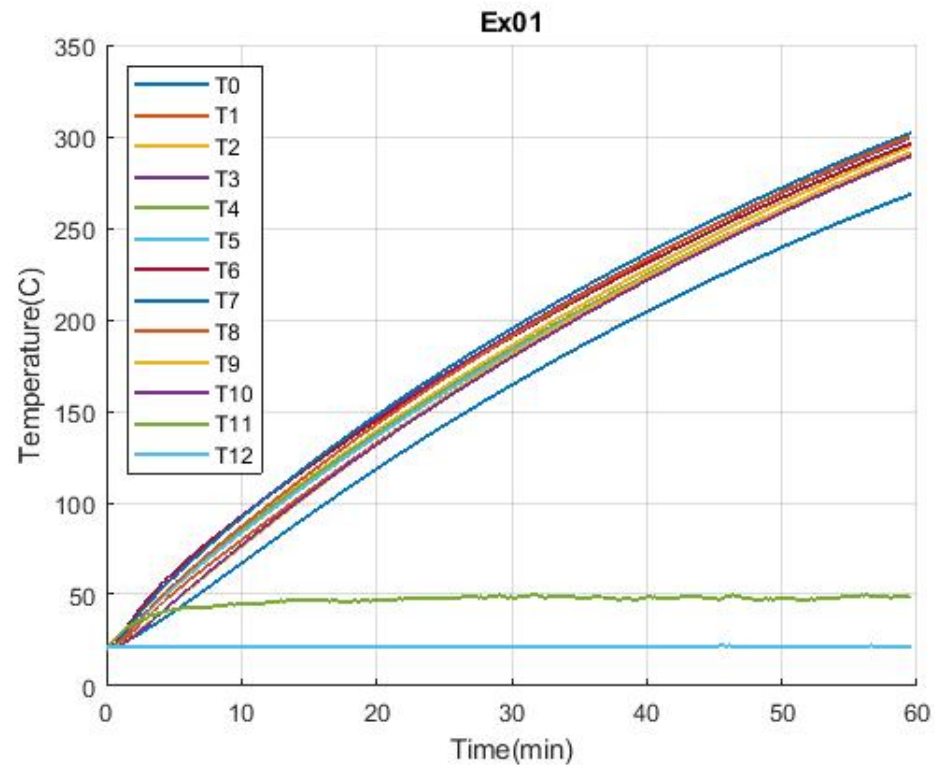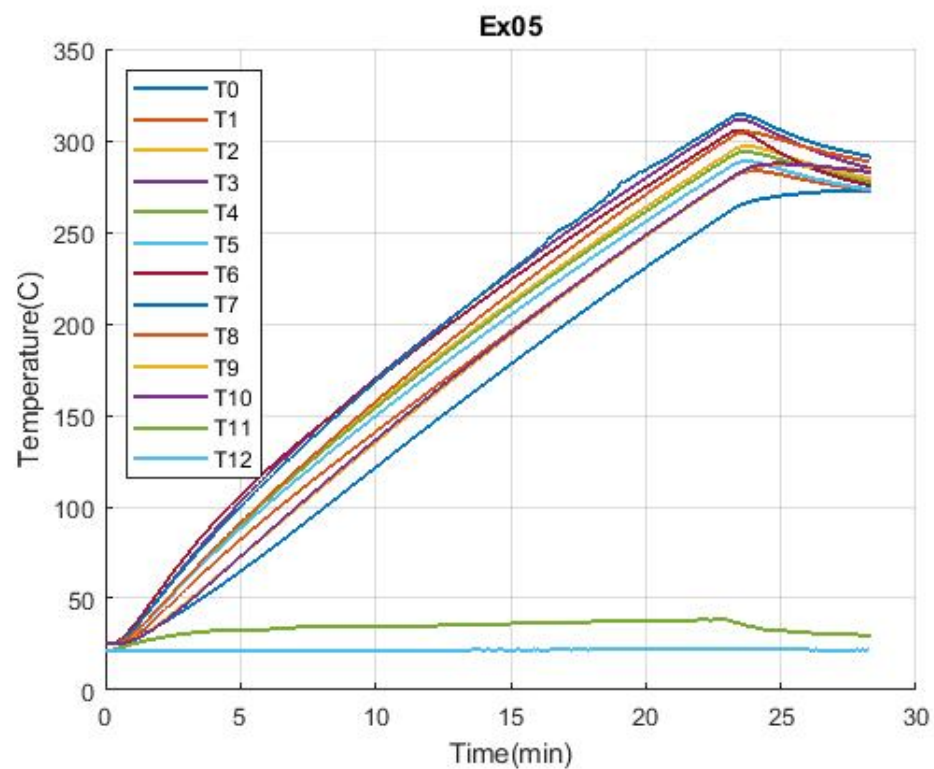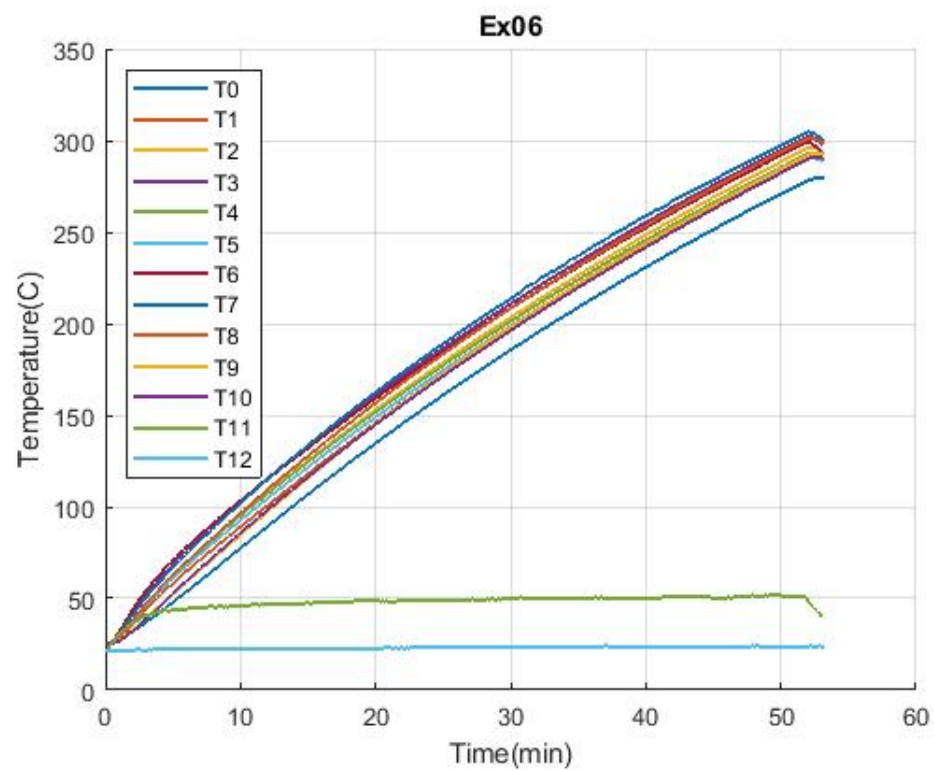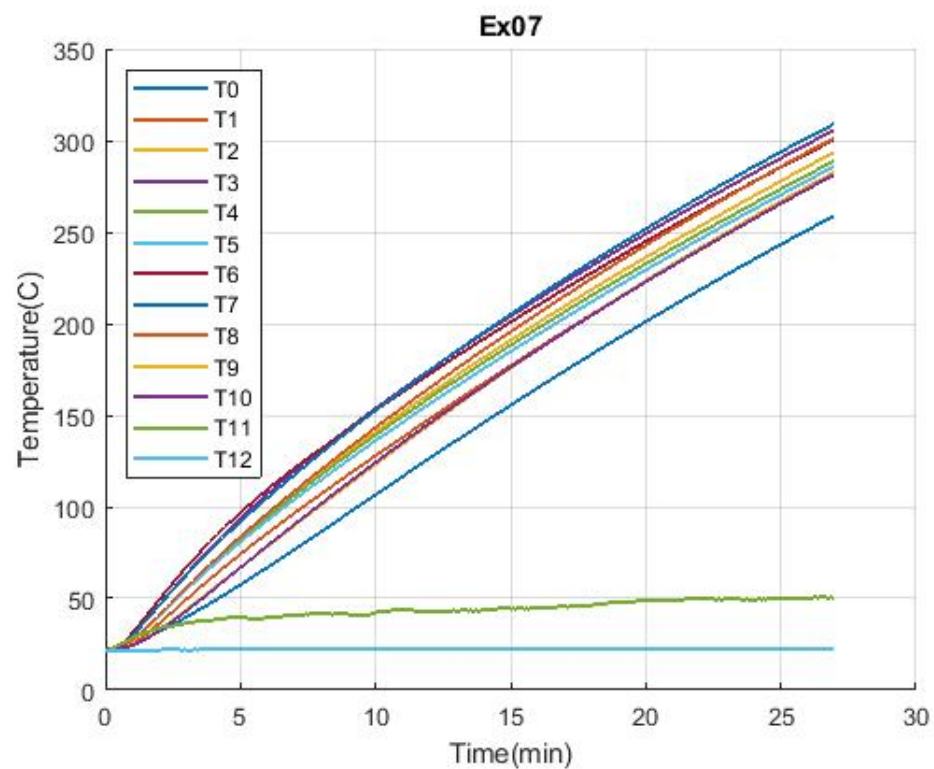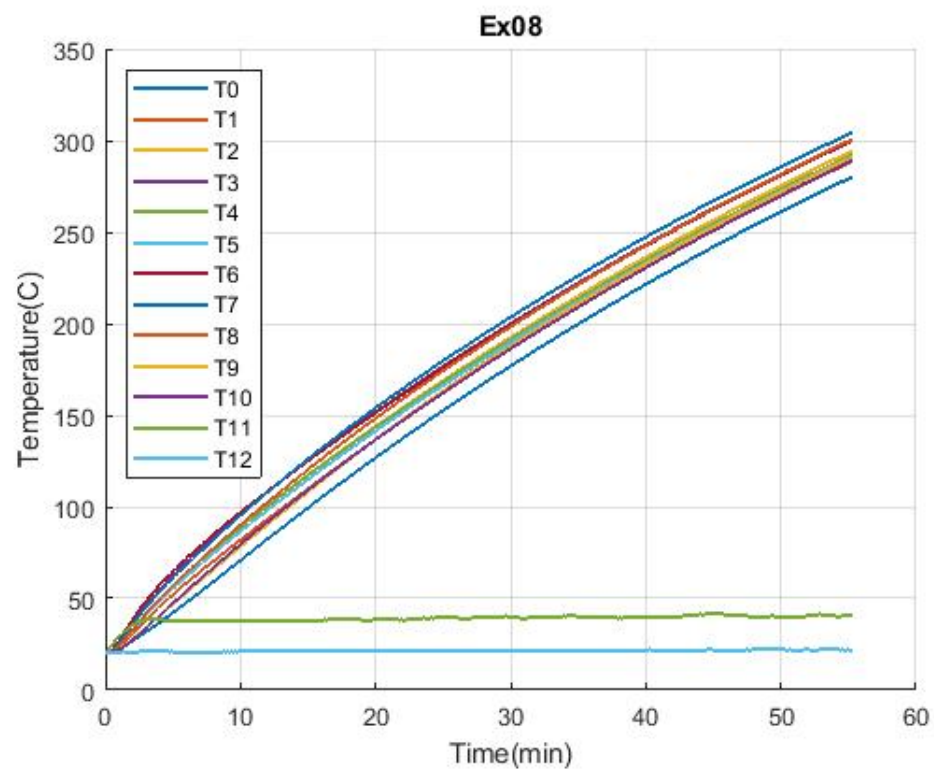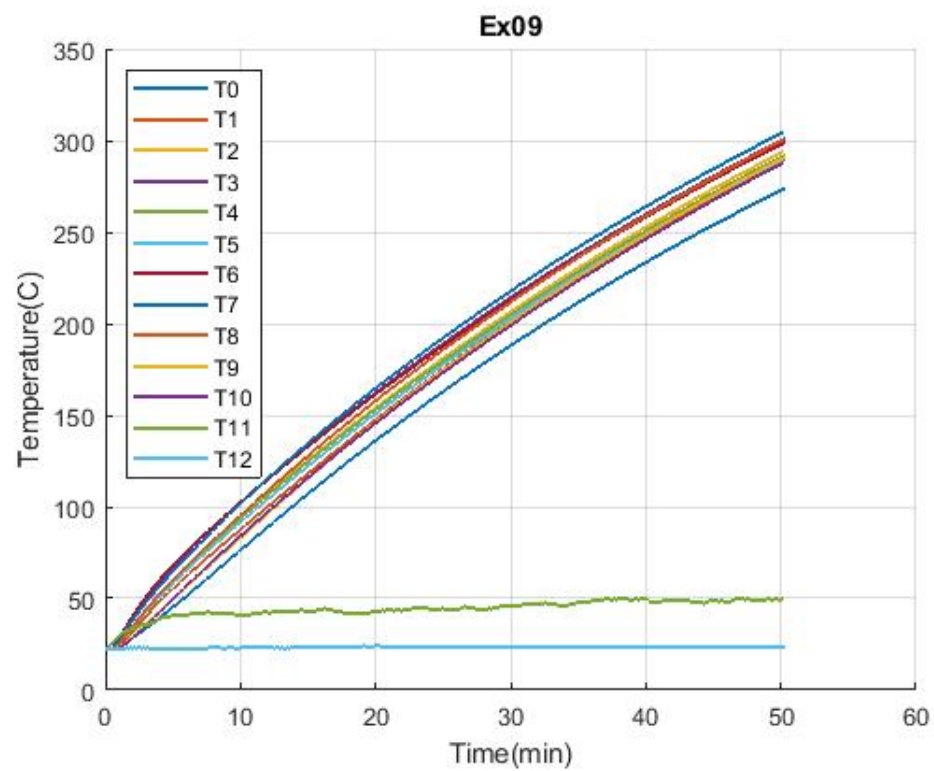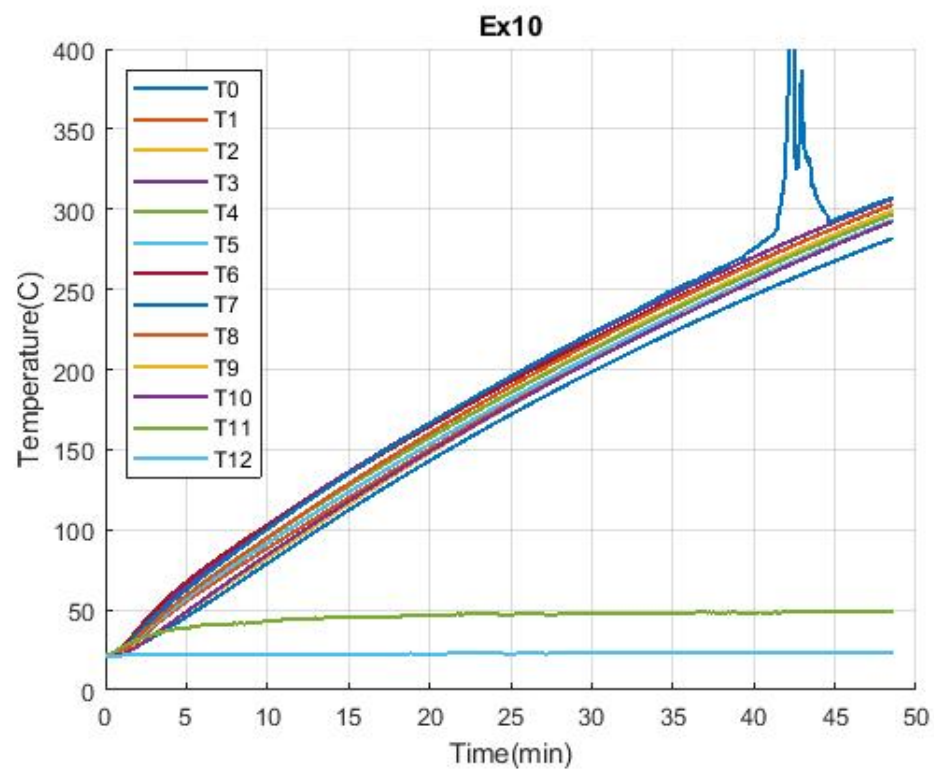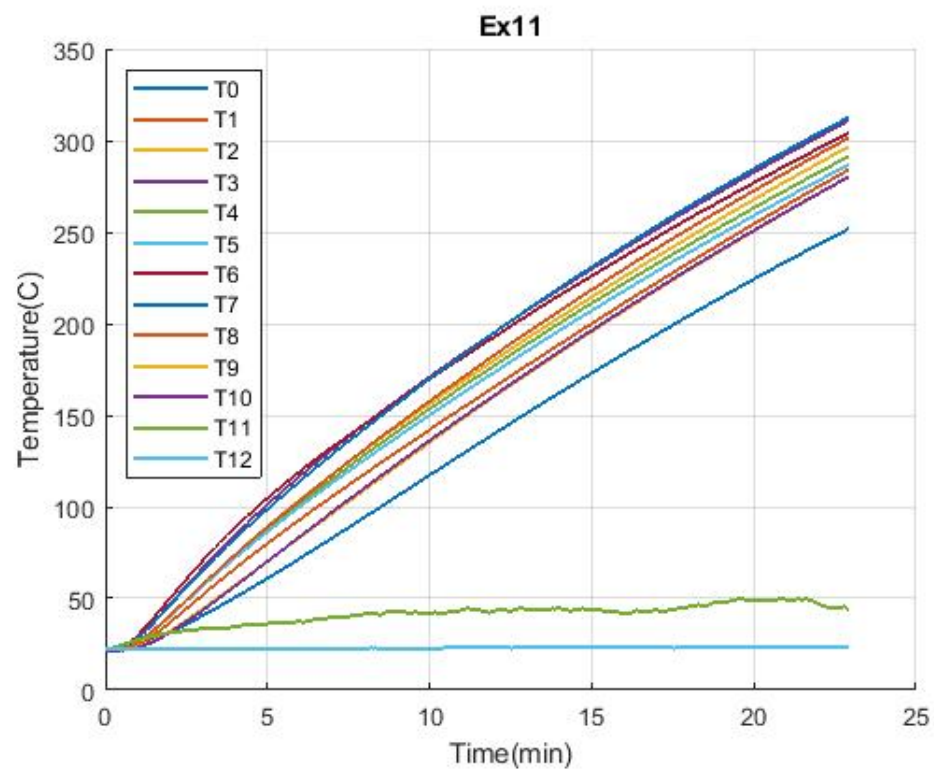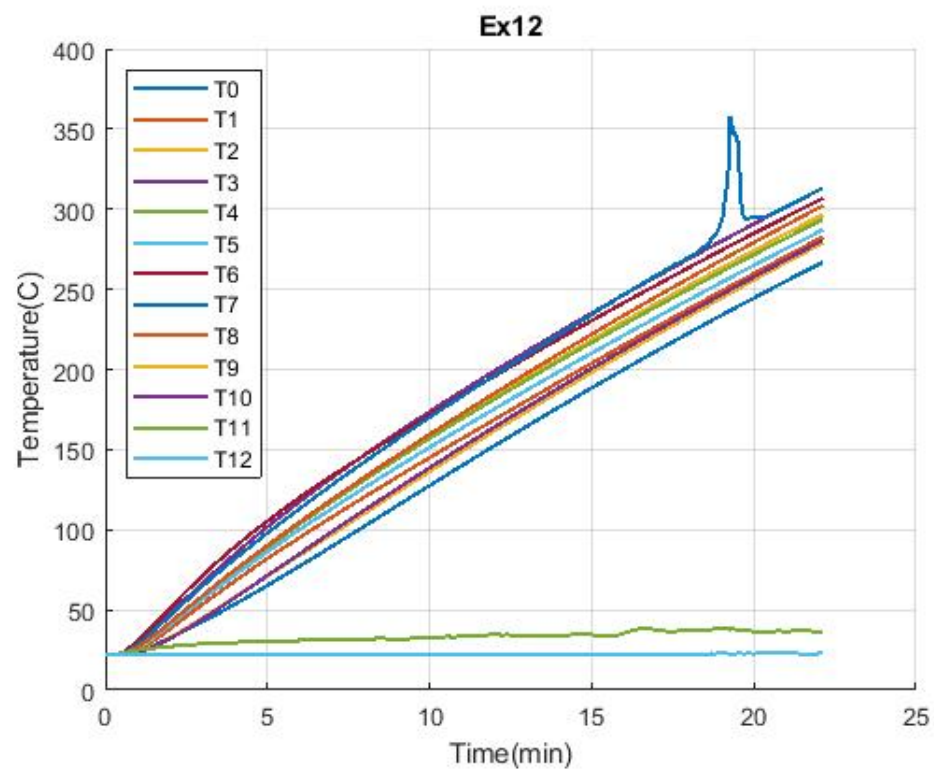

Figure A.1. Experiment 01 Heating Curves
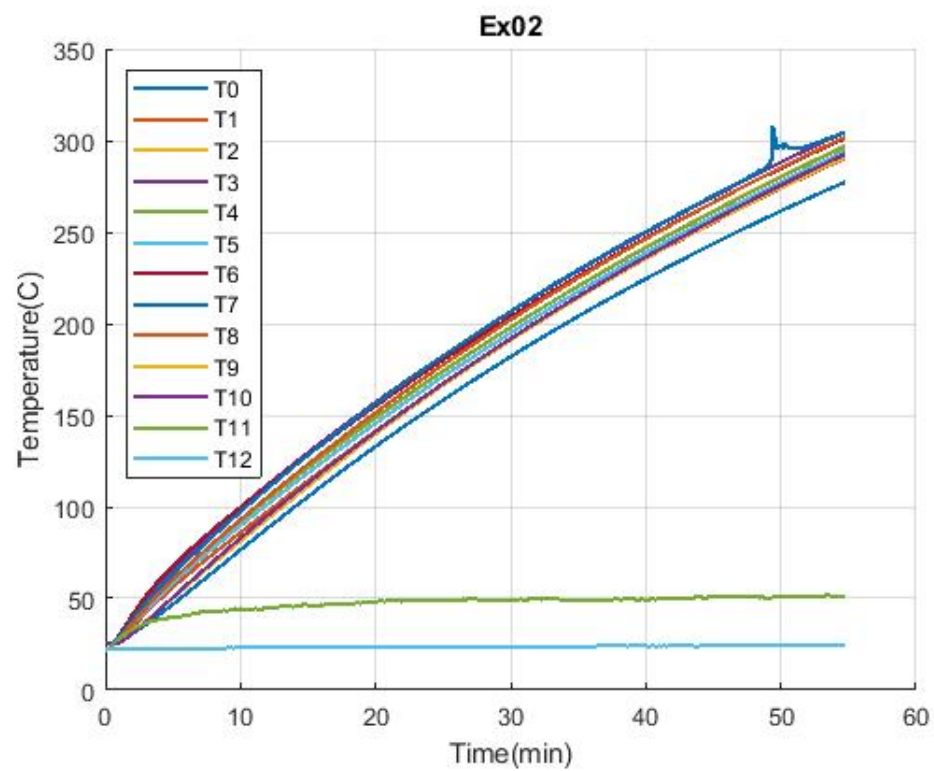
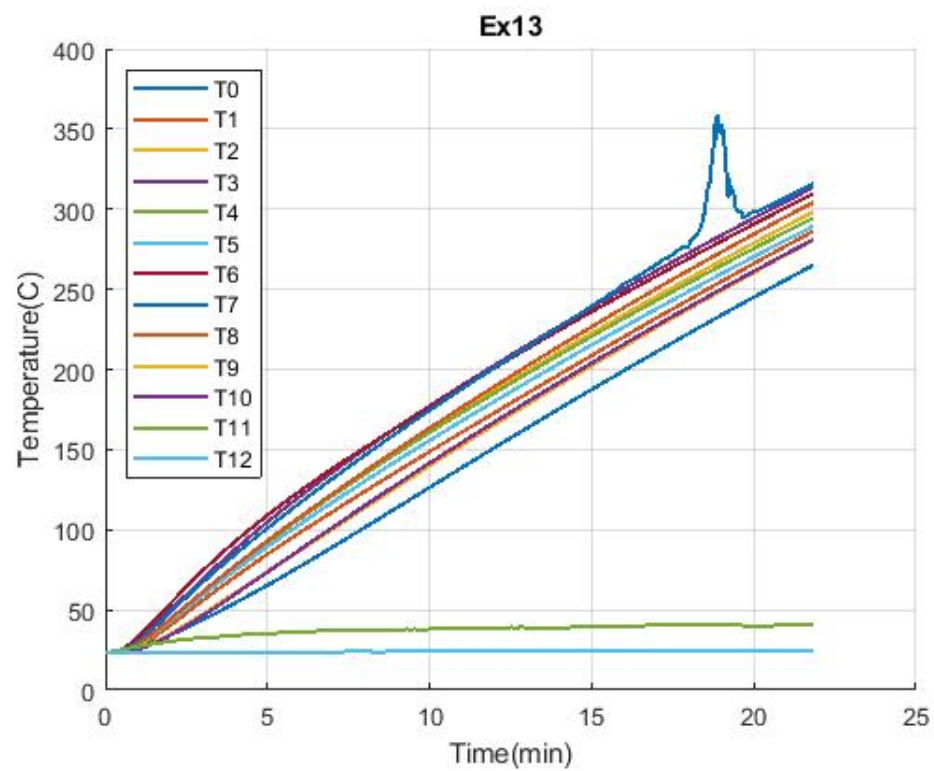*Figure A.2.* Experiment 02 Heating Curves
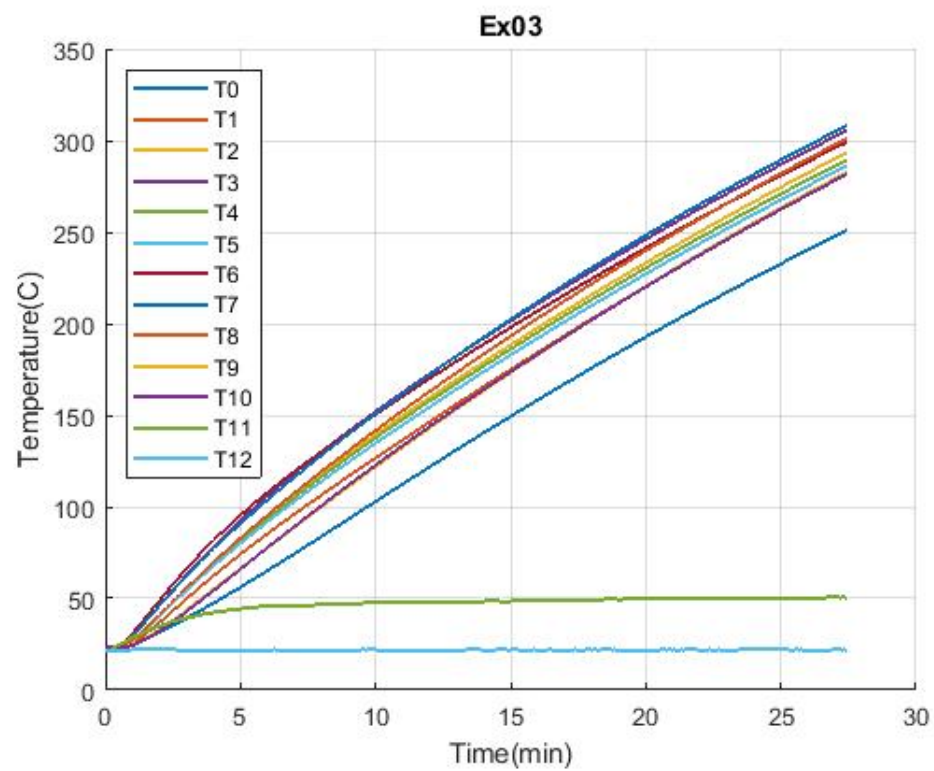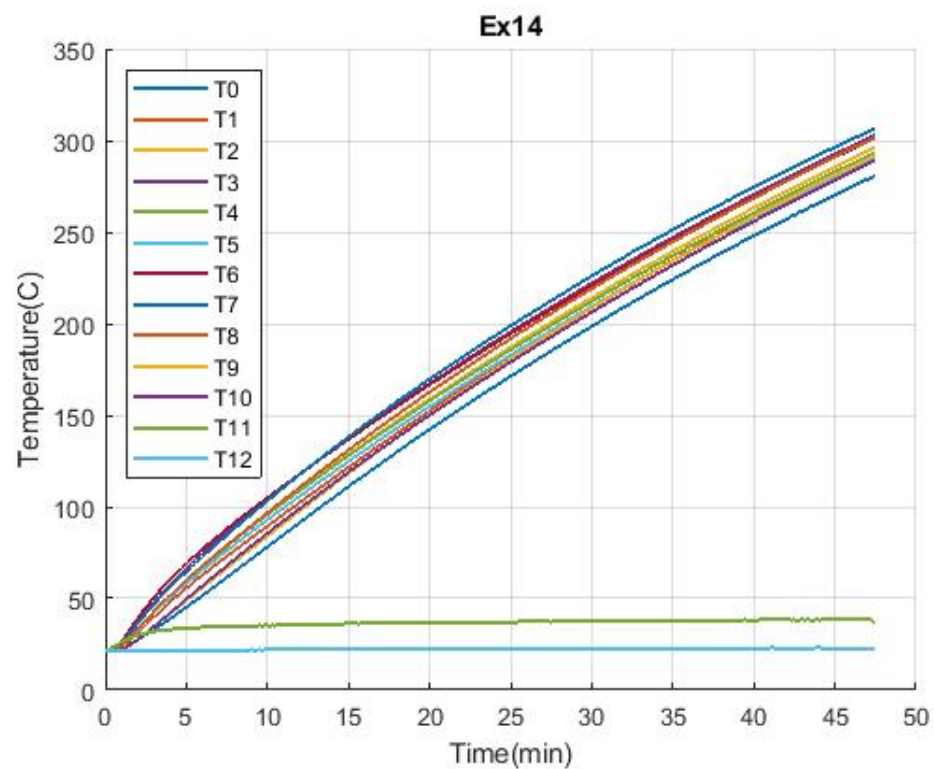
Figure A.3. Experiment 03 Heating Curves
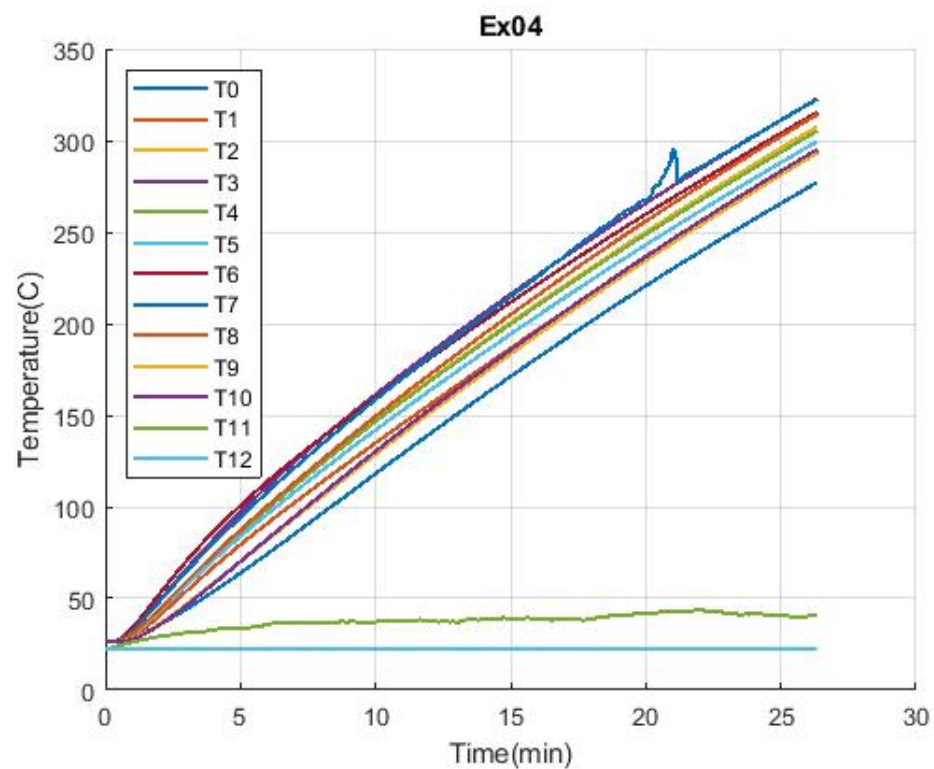
Figure A.4. Experiment 04 Heating Curves

Figure A.5. Experiment 05 Heating Curves

Figure A.6. Experiment 06 Heating Curves

Figure A.7. Experiment 07 Heating Curves

Figure A.8. Experiment 08 Heating Curves

Figure A.9. Experiment 09 Heating Curves

Figure A.10. Experiment 10 Heating Curves

Figure A.11. Experiment 11 Heating Curves

Figure A.12. Experiment 12 Heating Curves

Figure A.13. Experiment 13 Heating Curves

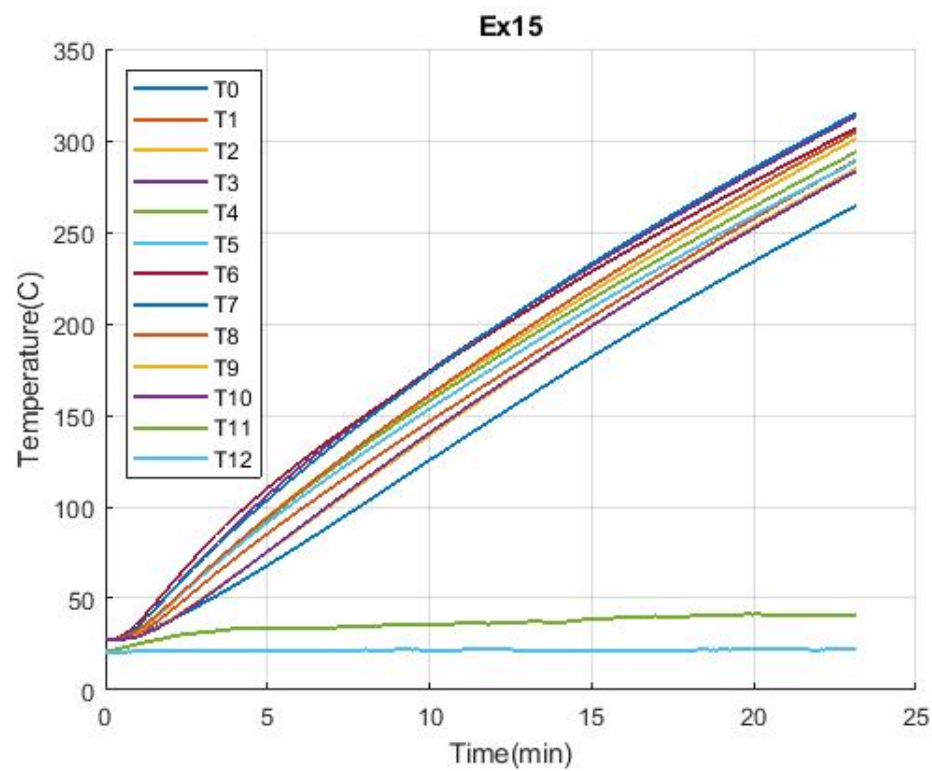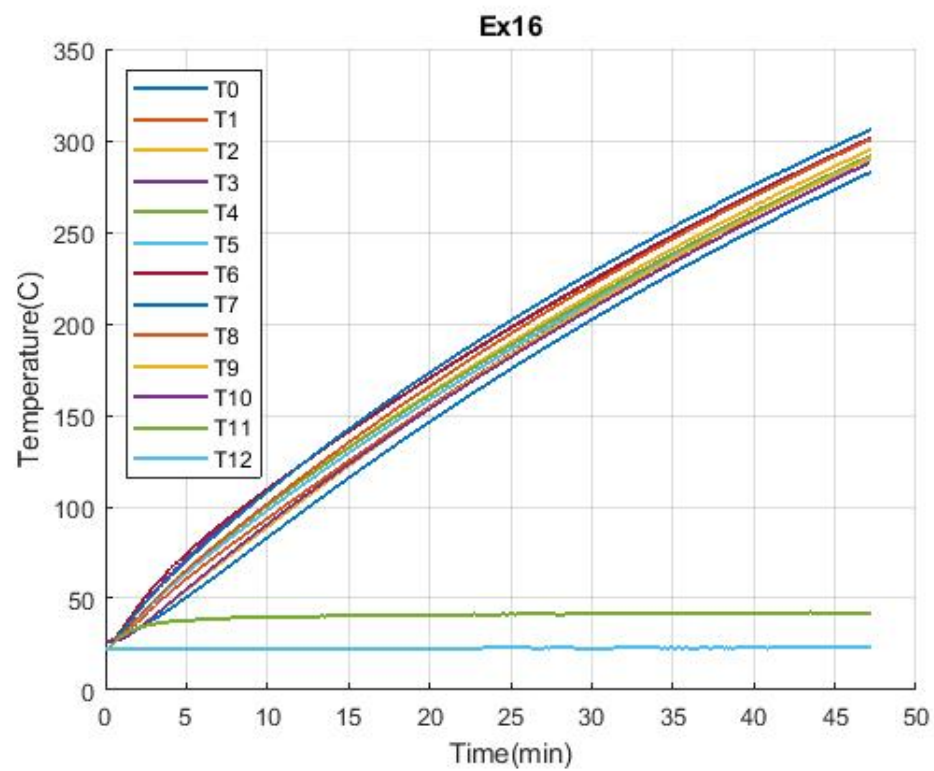*Figure A.14.* Experiment 14 Heating Curves

Figure A.15. Experiment 15 Heating Curves

Figure A.16. Experiment 16 Heating Curves